0. Executive Summary

Fibre-reinforced composites are instrumental for achieving a carbon neutral aviation. State-of-the-art composite airlines, such as the A350, burn approximately 20% less fuel than the previous generation. This is due to the weight savings achieved at airframe level, as well as by the adoption of fuel lean engines. However, the fuel efficiency of current high bypass ratio turbofans is largely due to the adoption of lightweight carbon-fibre composites in the fan system. Hence the adoption of composites has strongly benefitted both the airframe structures and the propulsive system.

The current design philosophy for the design of composites aero-structures is based upon a "no-growth" approach. This implies that composites in service may suffer from damage, for example due to impact, but the resulting flaws are not allowed to propagate into defects that may comprise the overall load-carrying capability. The "no-growth" paradigm is substantiated via extensive material and structural characterisations, following a "pyramid of testing" approach. Mechanical tests are therefore carried out at increasing level of complexity, starting from material coupons and progressing to components, elements and, finally, full airframes. The key objective of these characterisations is to obtain "design allowables", i.e. values of stresses and strains that must not be exceeded in service in order to meet the "no growth" criterion.

Environmental effects (i.e. temperature and humidity) strongly affect the mechanical performance of materials, hence the structural reliability in service. The definition of robust design allowables requires understanding and quantifying the effect of temperature and humidity on the mechanical performance of composites. Temperature affects the visco-elastic-plastic response of polymer matrices in fibre-reinforced composites. Increasing temperature promotes polymer creep and promotes an increase ductile behaviour of composite matrices. On the other hand, sub-zero temperatures tend to cause an embrittlement of the matrix, with associated micro-cracking. Humidity and the consequent moisture uptake cause swelling of the laminates and cause degradation of the fibre/matrix interface. Hence both temperature and humidity significantly affect the micro-structural behaviour of composites and are detrimental for long-term mechanical performance. In the context of "no growth" design, the role of environmental effects need to be accounted for when identifying "design allowables". Historically, "hot & wet" conditions have been considered the most detrimental for the mechanical performance of composites. However, composite structures in service are exposed to variable temperature and humidity. It is therefore crucial to establish

whether “environmental cycles” may accelerate the damage accumulation for composites in service. A typical civil airliner cruises at 35,000 ft at temperatures close to -50°C with negligible levels of humidity. On the other hand, landing at a tropical destination may expose the airframe to temperatures in excess of 50°C and 100% relative humidity. The actual severity of the environmental aging experienced by a composite aircraft is therefore a strong function of its operative history. Hence, “hot & wet” conditions do not necessarily constitute the worst-case scenario that has to be mitigated in design. It is necessary to consider the full possible environmental spectrum associated with in-service conditions. This implies the need for reliable methods to predict how damage evolves with varying environmental conditions.

This project has investigated the synergistic role of temperature and humidity on the mechanical strength of fibre-reinforced composites. Mechanical testing at different temperatures and moisture content provides “isolated” data points for finite sets of conditions. Albeit informative, these tests cannot cover the full spectrum of environmental scenarios experienced by an aircraft in service. Hence, the key objective of this project was to develop theoretical approaches and numerical tools that will allow extrapolating “design allowables” for arbitrary operational conditions from a sparse set of experimental data. The method applied to derive the “design allowables” is based on the time-temperature-humidity shift principle. This states that that the effects of temperature and humidity are equivalent to a scaling of the actual service life. A representative curve of the material strength as a function of time, also known as a master curve, can be obtained from tests at reference temperature and humidity conditions. The choice of the reference state is arbitrary, but in this research we considered 20°C temperature and 0% moisture content, i.e. nominally “dry” material. The actual strength of the material after a given time in service at a different temperature and moisture content level is then obtained from the master curve just by stretching or contracting the time axis. The entity of the deformation of the time axis is identified by creep tests performed on small coupons of material at prescribed set of temperature and humidity. The advantage of this approach is that all the matrix dominated properties scale according to the master curve generated by the creep tests. There is no need for performing tests at every possible temperature and humidity on coupons having different configurations depending on the mechanical strength property that is considered. A much smaller set of tests is generally performed with the aim of validating the time-temperature-shift principle, so that a smooth mapping relating different environmental conditions is obtained from a relative small set of data. The advantage of this approach is that the operative life of a component can be estimated by accumulating the time fractions spent in each service condition in a linear

fashion, not dissimilarly from what done when using the Miner's rule in fatigue analysis. Moreover, the amount of testing that is required for substantiating a "no growth" design in presence of environmental effects is dramatically reduced, and this is highly beneficial in terms of costs.

In this project, the time-temperature-shift principle has been validated for a carbon fire-reinforced epoxy material, namely Cytek Cycom 977-2. This material is extensively employed in primary aeronautical structures, such as fuselages and wings.

The creep response of the material has been characterised at temperatures below the grass transition (180°C) via tests performed in a dynamical mechanical analyser. Master curve of the creep storage modulus have been obtained for both dry and fully saturated specimens. The strength of the material in tension and compression has been characterised via ASTM standard coupons, considering a wide range of service temperatures, for both dry and fully saturated coupons. It has been demonstrated that the master curves obtained for the storage modulus allow predicting the strength of the material in the full range of environmental conditions considered. These results have also been extended to the prediction of the effect of the strain-rate on the strength, which is extremely important for design purposes. The key outcome of this research is that the visco-elastic response of the material has a massive impact on the strength and that environmental effects strongly influence the visco-elastic response. It has also been observed that the shift factor associated with temperature and humidity can be suitably described by characteristic activation energies, which are inherent material properties. The residual strength properties of the fully saturated material have been found to be extremely low, particularly in terms of transverse tension. This poses significant challenges for the design of composite structures in service and highlights the importance of predicting/monitoring the actual moisture content in service, as well as inhibiting the moisture ingress in composite materials via suitable surface protections (i.e. paints).

Future work for assessing the real hazard posed by environmental factors on the durability of composites in service will have to be focussed on the characterisation/prediction of the effects of cyclic temperature and moisture. This project has proven the viability of the time-temperature-humidity shift principles for steady environmental conditions, but it remains to be demonstrated whether the same approach holds for materials that experience cyclic environmental regimes. The data gathered and the analysis methods developed in this project provide a rationale scientific basis for the extension of the time-temperature-humidity shift method to variable temperature/humidity scenarios.

1. Experimental Data

1.1.1 Introduction and Background

Fibre Reinforced Plastics (FRP) have excellent specific strength and stiffness and are therefore employed in primary and secondary load carrying structural members in airframes. The development of testing procedure to evaluate the lifetimes of composites in service conditions is getting increasing attention, due to the need of ensuring long-term durability of structural component. The demanded service life of composites in many applications is long and mechanical properties are expected to change over that time. For example, in high-speed (cruise at Mach 2) commercial aircraft, the material is required to last for 20 years, with 60,000 hours spent at elevated temperature [1]. It is clearly impractical to run tests than span the entire service life, under a variety of environmental conditions that involve both temperature and humidity cycles. Even if such long tests could be performed, considering advances in technology, the materials that will be employed 20 years from now are likely to be completely different from those that one might start testing today. For these reasons, accelerated testing methodologies able to account for environmental degradation are needed for the certification of primary composites aerospace structures.

S-N curves, whereby fatigue strengths are expressed as functions of the number of fatigue cycles, are the most commonly employed tool to predict the endurance of allots. Acceleration of fatigue in alloys is accomplished by increasing the frequency of loading. Haskins and Kerr [2] used this technique to reduce test times by a factor of 120. This approach generally works well, as long as other time-dependent phenomena, such as viscoelasticity or oxidation, do not influence with the fatigue response. Unlike metals, the stress-strain relations of polymeric matrices exhibit strong viscoelastic (time and temperature dependence) behaviour, not only above the glass transition temperature Tg, but also below Tg. Since time plays a major role in the fatigue and creep of polymer composites, S-N curves cannot provide accurate predictions of the actual fatigue life. Accelerated testing of viscoelastic deformation is well established, and usually accomplished using time-temperature superposition principle (TTSP) [3]. Here elevating the temperature is used to effectively accelerate time. Acceleration of chemical degradation, such as oxidation in alloys or UV degradation of polymers is more difficult, albeit possible since temperature influences the reaction kinetics. The main issue with any accelerating scheme is clearly establishing the relationship between the accelerated test and the actual service life.

Regarding the time-temperature shift factor, compliance measurements are made over a short time period at several different temperatures. These compliance measurements are plotted against the log of time. It has been found that the compliance measurements can be shifted on the log time scale to form a smooth trend called a master curve, as shown in Figure 1. This curve predicts the compliance of the material over a larger time range than that actually tested. The amount of acceleration provided by a given increase in temperature is established by the overlapping of the compliance curves measured at the different temperatures [1].

To form the master trend, one curve, corresponding to an arbitrary reference temperature, remains stationary, while all the other curves are shifted towards the reference. The temperature for which the master curve predicts time-dependent deformation is the reference one. By recording the time shifts required to form the master curve, commonly referred to as shift factors, a relation between the horizontal shifts and temperature is established. This relationship can be used to shift the entire master curve to other temperatures. Using the master curve shifted to the appropriate temperature, creep compliance over many orders of magnitude can be predicted. The time temperature superposition principle (TTSP) was originally developed to account for the influence of viscoelasticity on stiffness properties, but it has been successfully extended to predict the strength of polymeric matrix composites [4-8]. Models the dependency of the shift factor on temperature have also been developed, albeit an Arrhenius law is usually appropriate for this purpose.

Miyano and Nakada [9-10] measured tensile strength of resin impregnated carbon fibre strands under various constant strain-rates (CSR) and temperatures. They plotted the tensile strength against failure time in logarithmic scale for each test temperature. They constructed a master curve of tensile strength indicating the validity of the time-temperature superposition principle. It is worth noting the shift factor for the tensile strength was almost coincident with that for storage modulus of the matrix resin.

Miyano et al [11] also measured the compressive strength of resin impregnated carbon fibre strands under various constant strain-rates (CSR) and temperatures. Using the same procedure for the tensile strength as in [9-10], they constructed master curve of compressive strength which indicated the validity of the time-temperature superposition principle. Using the Rosen's strength formula [12-13] for fibre reinforced composite with elastic matrix, Miyano et al [11] predicted the tensile and compressive strengths along the longitudinal direction of unidirectional CFRP under CSR loading.

1.1.2 DMA Testing

A Dynamic Mechanical Analyser (DMA) with a 3-point bending fixture is used for carbon-fibre reinforced epoxy Cycom 977-2 coupons. Dry as well as fully saturated CFRP coupons were tested. The coupons were 1 *mm* thick, 15 *mm* wide and 50 *mm* long. The testing time was kept 2000 seconds for dry as well as saturated test coupons except 130 °C for dry coupon. The tests were run for 20000 seconds, but after 3836 seconds maximum the load drop was beyond what could be recorded with the DMA setup, as shown in Figure 1. Dry coupons were tested at a room temperature (RT), 60 °C, 80 °C, 100 °C, 120 °C, 130 °C, 150 °C, 160 °C, 170 °C and 180 °C, as plotted in Figure 1. Saturated (wet) coupons were tested at a room temperature (RT), 40 °C, 50 °C, 60 °C, 70 °C, 80 °C, 90 °C, 100 °C, 110 °C, 120 °C, 140 °C, 145 °C, 150 °C, and 160 °Cm as plotted in Figure2. It is clear that wet/saturated samples have lower storage modulus compared to dry coupons for almost all of the temperature tested

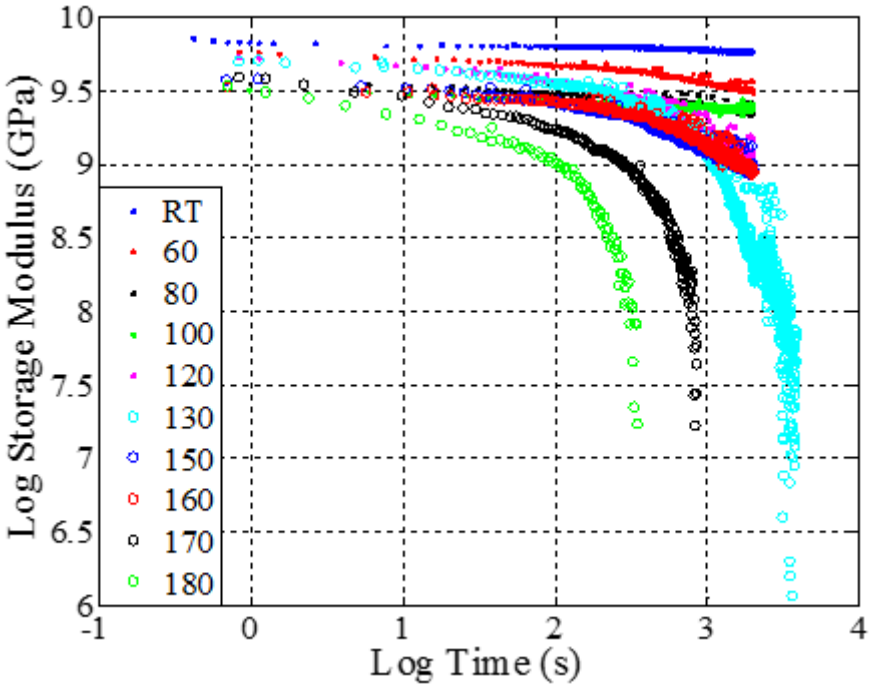

Figure 1. Individual plots for different temperature ranges for dry CFRP coupons

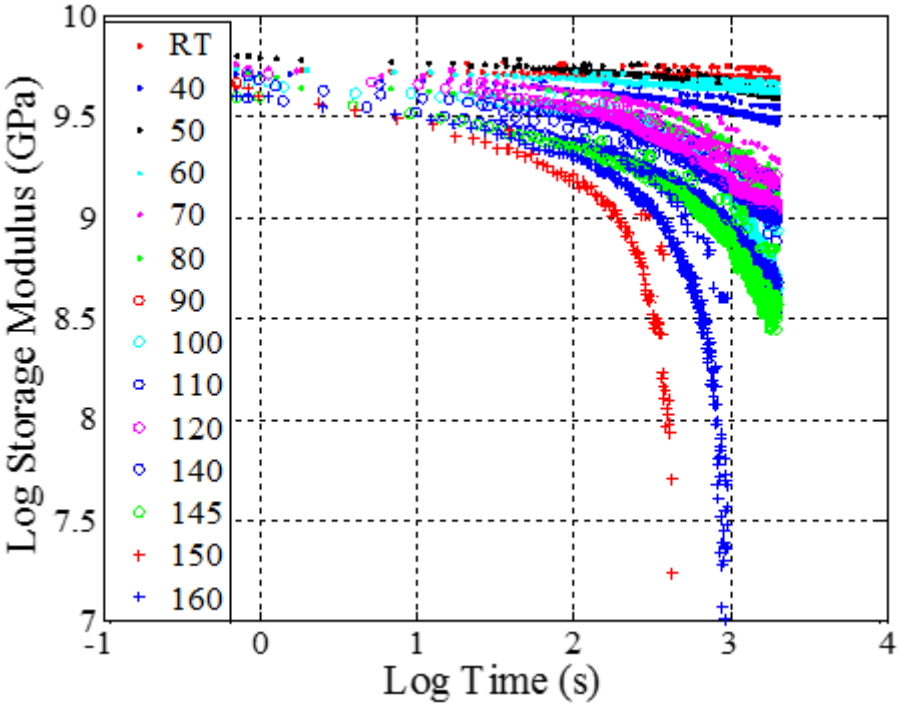

Figure 2. Individual plots for different temperature ranges for saturated CFRP coupons

A Matlab routine was programmed for plotting the master curve making use of "nlinfit" command which estimates the coefficients of a nonlinear regression function, using the least squares method. The master curves are presented in Fig. 3 and 4. The experimental data conform very well to the master curve for dry and wet CFRP samples.

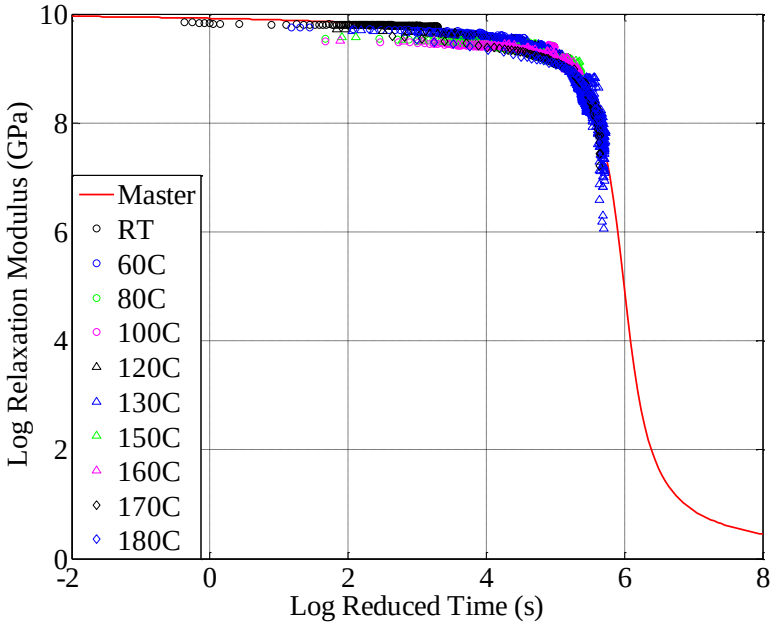

Figure 3. Master Curve of storage modulus of dry CFRP coupons

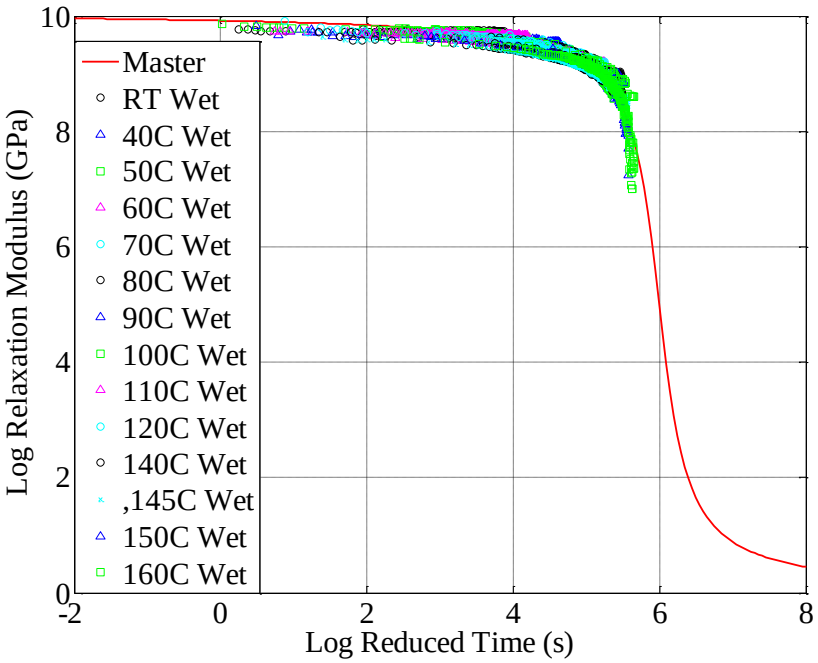

Figure 4. Master Curve of storage modulus of Wet CFRP coupons

1.2 Tensile Testing

1.2.1 Manufacturing of Specimens

As mentioned before, the material characterised in this study is Cytek Cycom 977-2. The composite is made of intermediate modulus carbon fibres IM7, with 12k fibre count, and 977-2 epoxy matrix. The latter is toughened with thermoplastic material. Cycom 977-2 is routinely used in primary and secondary aerospace structures. ASTM D3039 standard coupons were manufactured in order to carry out mechanical characterisation pre- and post-exposure. For the end tabs, both AS4/8552 and E-glass4/8552 were used, as the supply for the former was delayed in the laboratory and the latter was ordered instead.

The lay-up angles, 0^o, $\pm 45^o$ and 90^o, reported refer to the fibre orientation with respect to the coupon longitudinal axis. After manually laying up the $[0]_4$, [±45] and [90] layups, the laminates were cured in autoclave. A diamond saw was used to cut the laminate panels into required specimen sizes. The specimen dimensions used for the mechanical testing are summarised in table 1 and are also shown in Figures 5-7. Grit blasting was carried out to prepare the surfaces for the composite and end tab better joint. After grit blasting, acetone was used to clean the surfaces. Care was taken to avoid reinforcing fibres being exposed or damaged as a consequence of grid blasting. In order to bond the tabs to the coupons, a two-

component, high-strength, paste epoxy-based adhesive was used, namely Letoxit LH 149. 100 weight parts of A component (thixotropic paste of yellow colour) with 40 weight parts of B component (fluid of blue colour) were mixed thoroughly until an even colour shade is achieved. After this, the adhesive was applied to both surfaces to be bonded. The adhesive bond line thickness varied in the range 0.1-0.2 *mm*. The bonded parts were cured for 4 hours at 50 °C in an oven.

Table1. Tensile Specimen Geometry

Fibre Orientation	**Width (*mm*)**	**Overall Length (*mm*)**	**Thickness (*mm*)**	**Tab Length (*mm*)**	**Tab Thickness (*mm*)**	**Tab Bevel Angle**
0^o	15	250	0.82	60	2	90
$\pm45^o$	15	250	2	60	2	90
90^o	15	175	2	30	2	90

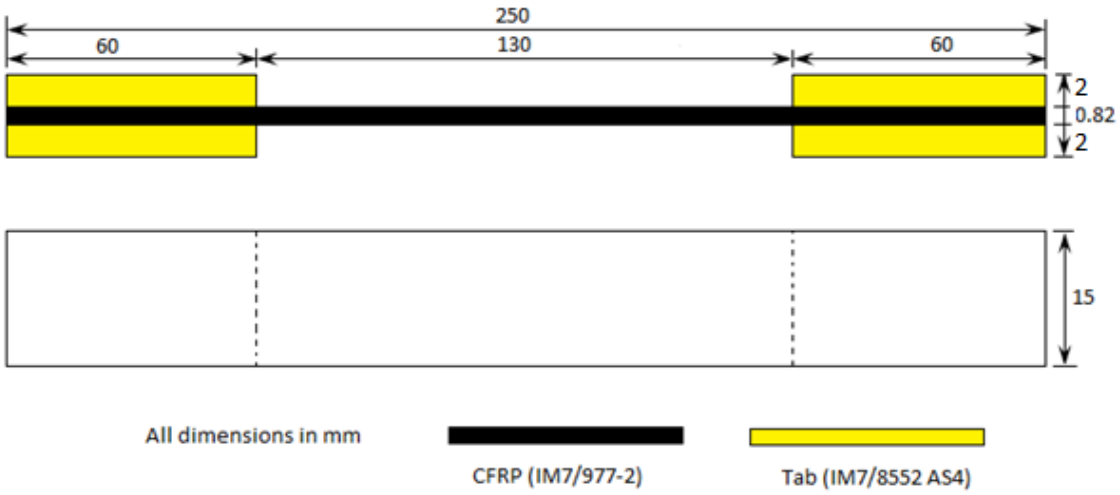

Figure 5. Typical specimen used for 0^o unidirectional layup

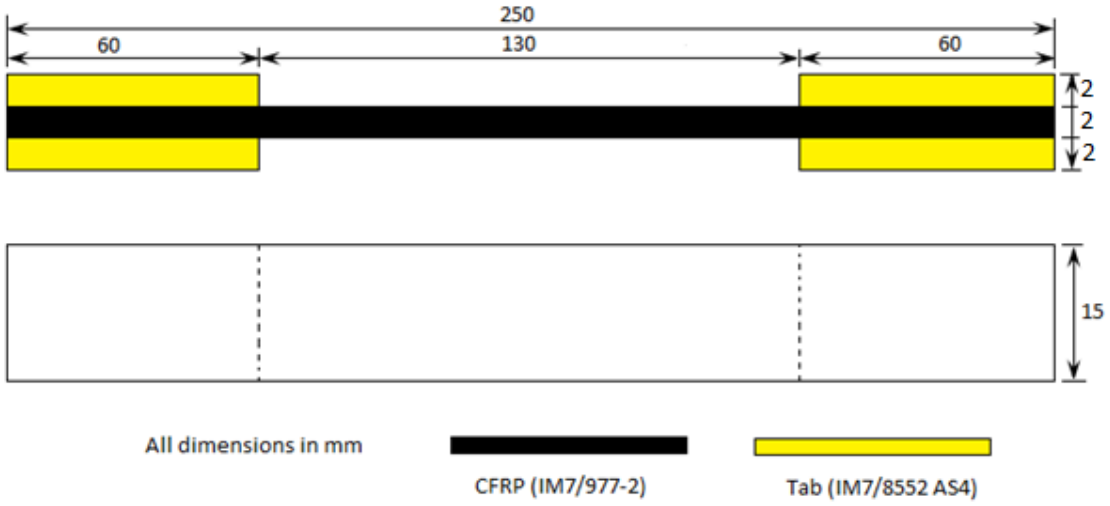

Figure 6. Typical specimen used for ±45^{o} unidirectional layup

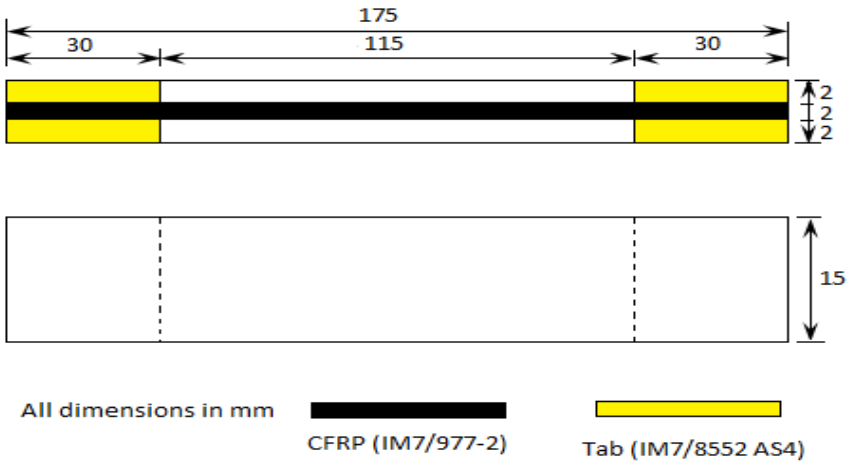

Figure 7. Typical specimen used for 90^{o} unidirectional layup

1.2.2 Humidity Conditioning

Specimens were put in the water bath and the progress of moisture ingress in the composites was monitored, as shown in Figure 8. The water temperature was initially kept at room temperature; then it was raised to *80 ^{o}C* to characterise the change of humidity absorption rate in the samples. The increase of the water temperature accelerated the moisture uptake process as expected. To reduce the evaporation rate from the water bath, lightweight, economic polypropylene anti-evaporation spheres were used. The spheres were used as these reduce heat loss by approximately *77*% and evaporation by *87%*. The bath was further covered with metallic lid to avoid any external contamination. The coupons aged in the water bath were: 8 unidirectional *0*^{o}, 12 cross-ply and 8 unidirectional *90*^{o} . The *±45*^{o} and *90*^{o} specimens were placed in the water bath on *29*th November, 2013 and were tested on 25th February, 2014 at

room temperature conditions and on *5th* and *6th* March, 2014 at *80 °C*. The 0^o layup specimens were placed in the water bath on *8*th February, 2014 and were tested on 14th March at room temperature conditions and on *17th* March, 2014 at *80 °C*. The reason for this delay in ageing the *0o* layup specimens was that the failure load of 2mm thick coupons was found to be approximately *70kN*. At this load level, a very high clamping pressure had to be applied to the hydraulic grips in order to avoid slippage of the coupon during the test. This cause premature failure of the coupon close to the end tabs, which does not constitute a valid failure mode for tensile strength characterisation. Therefore the thickness of *0o* unidirectional coupons was reduced to 4 plies only, for a 0.82 mm thickness after curing. The water bath temperature for the second batch *0o* unidirectional coupons of was kept at *80°C* . The weights of the specimens were measured before the immersion in the water bath and then daily throughout the conditioning period. A summary of the weight variation for all the specimens exposed is presented in Table 2-4. Due to the small thickness of the coupons, the moisture ingress took place mainly from the top and bottom surfaces in the gauge section. It is expected that the material within the tabbed region was not saturated due to the presence of the tabs themselves.

Figure 8. Water bath to moisture the specimens

Table 2. Moisture gain for 0^o orientation specimens

Fibre Orientation	Dry Specimen Weight(*gms*)	Weight before Testing (*gms*)	Moisture Contents (*gms*)	Moisture contents (*%*)
0^o	14.069	14.307	0.238	1.69
0^o	13.301	13.476	0.175	1.32

0^o	14.153	14.411	0.258	1.82
0^o	14.011	14.232	0.221	1.58
0^o	14.106	14.296	0.19	1.35
0^o	14.159	14.352	0.193	1.36
0^o	13.869	14.07	0.201	1.45
0^o	14.104	14.325	0.221	1.57

Table 3. Moisture gain for ±45^o orientation specimens

Fibre Orientation	**Dry Specimen Weight(*gms)***	**Weight before Testing (*gms*)**	**Moisture Contents (*gms*)**	**Moisture contents (*%)***
$\pm 45^o$	25.118	25.492	0.301	1.99
$\pm 45^o$	25.265	25.568	0.273	1.08
$\pm 45^o$	25.584	25.869	0.279	1.09
$\pm 45^o$	25.334	25.637	0.301	1.19
$\pm 45^o$	25.627	25.972	0.297	1.16
$\pm 45^o$	25.693	26.052	0.308	1.2
$\pm 45^o$	25.602	25.905	0.287	1.12
$\pm 45^o$	25.454	25.734	0.275	1.08
$\pm 45^o$	24.897	25.224	0.337	1.36
$\pm 45^o$	25.12	25.427	0.306	1.22

$\pm 45^o$	25.52	25.874	0.345	1.35
$\pm 45^o$	25.208	25.537	0.328	1.30

Table 4. Moisture gain for 90^o orientation specimens

Fibre Orientation	**Dry Specimen Weight*(gms)***	**Weight before Testing (*gms*)**	**Moisture Contents (*gms)***	**Moisture contents (*%)***
90^o	15.079	15.229	0.150	0.99
90^o	15.053	15.211	0.158	1.05
90^o	15.159	15.310	0.151	1.00
90^o	15.259	15.426	0.167	1.09
90^o	14.063	14.236	0.173	1.23
90^o	14.933	15.107	0.174	1.17
90^o	15.155	15.316	0.161	1.06

1.2.3 Mechanical Testing at Room Temperature

Specimens were mounted in the fixture of a servo-hydraulic mechanical testing machine and monotonically loaded in tension, while recording load. The tests were performed at a rate of 0.02 *mm/s*. The tests were repeated for a minimum of 3 times for each set of environmental ageing conditions. The hydraulic machine, as shown in Figure 9, had a 100 *kN* load capacity. The pressure on the 0^o and $\pm 45^o$ orientation specimens were kept to *2* bar to avoid the slippage of the specimens during the testing, while the pressure was reduced to *0.5* bar for 90^o orientation specimens to avoid failure in the tab section. The grips in the machines are self-aligning and lightly serrated to minimise bending stresses in the specimens. The tests confirmed that the specimen failure occurred within the coupons gauge section.

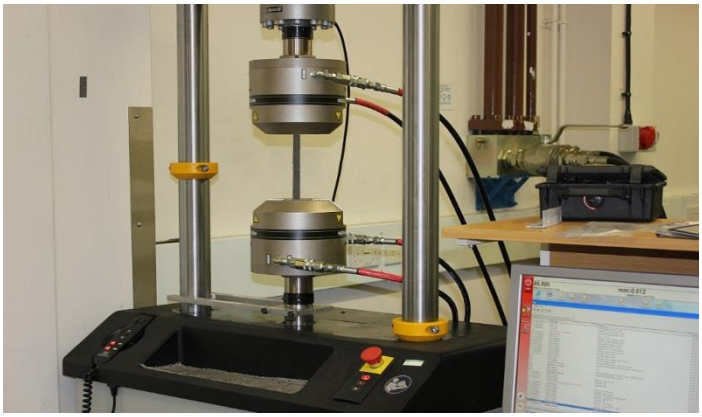

Figure 9. Machine used for the specimens testing at room temperature

1.2.4 Room Temperature Tests at 0^o Orientation

Dry and wet (moist) specimens were considered at room temperature for the 0^o orientation. Figures 10 and 11 show the load versus displacement plots for dry and wet specimens with 0^o orientation, while the failed specimens are shown in Figures 12 and 13, respectively. It is worth noting that the two different colours for the end tabs shown in the figures depend on the different tab material used, as outlined in Sec. 3.1. The right end of the specimens presented in the figures was gripped to the stationary machine head (top), while the left end was clamped to the movable head (down). This applies to all the specimens presented in this study. Results for the dry and wet conditions are summarised in Table 5 and 6 respectively.

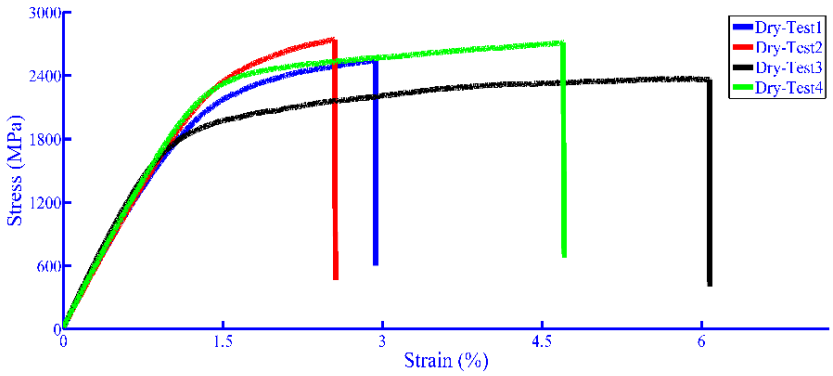

Figure 10. Dry tests for 0^o orientation at room temperature

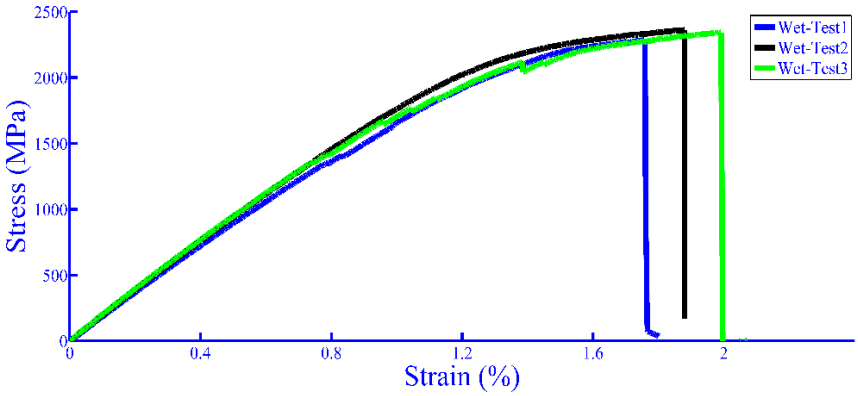

Figure 11. Wet tests for 0^o orientation at room temperature

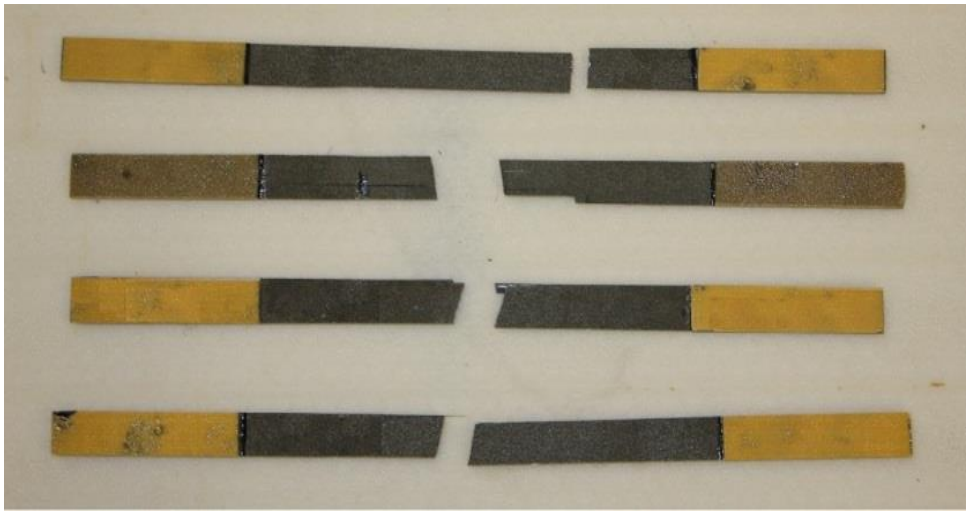

Figure 12. Failure surfaces of 0^o orientation specimens for dry test at room temperature

Figure 13. Failure surfaces of 0^o orientation specimens for wet test at room temperature

Table 5. Summary of dry test data for 0^o and Room Temperature

Fracture Load *kN*	Strength *MPa (ksi)*	Mean *MPa(ksi)*	Modulus *GPa (Msi)*	Mean *GPa (Msi)*
31.26	2541.11(368.56)	2590.71(375.75)	162.35 (23.55)	163.21(23.67)
33.72	2741.82(397.67)		166.61(24.17)	
29.14	2369.05(343.60)		162.02 (23.50)	
33.34	2710.86(393.18)		161.84 (23.47)	

Table 6. Summary of wet test data for 0^o and Room Temperature

Fracture Load *kN*	Strength *MPa (ksi)*	Mean *MPa(ksi)*	Modulus *GPa (Msi)*	Mean *GPa (Msi)*
28.13	2287.29(331.74)	2341.36(339.58)	160.93(23.34)	169.14(24.53)
29.04	2361.33(342.48)		171.87(24.93)	
29.22	2375.44(344.53)		174.61 (25.32)	

1.2.5 Room Temperature Tests at $\pm 45^o$ Orientation

Dry and wet (moist) specimen were considered for room temperature tests for the $\pm 45^o$ orientation. Figures 14 and 15 show the plots for dry and wet specimens at $\pm 45^o$ orientation, while the failed specimens are shown in Figures 16 and 17 respectively. Results for the dry and wet conditions are also summarised in Table 7 and 8 respectively.

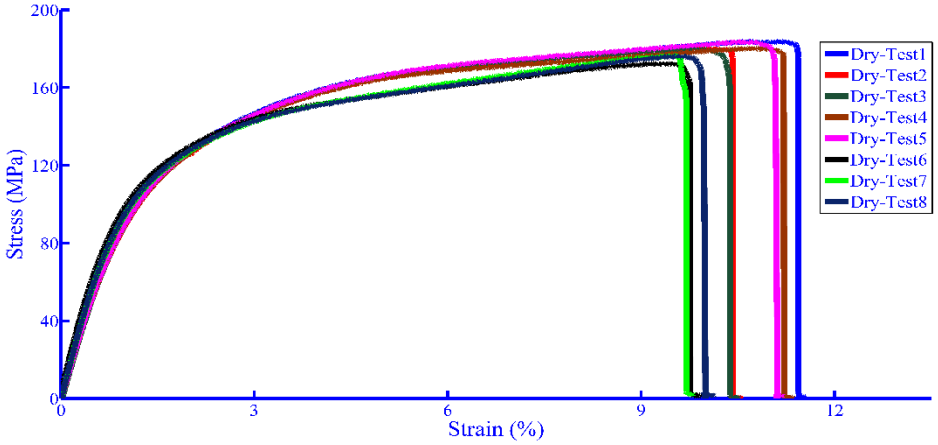

Figure 14. Dry tests for ±45^{o} orientation at room temperature

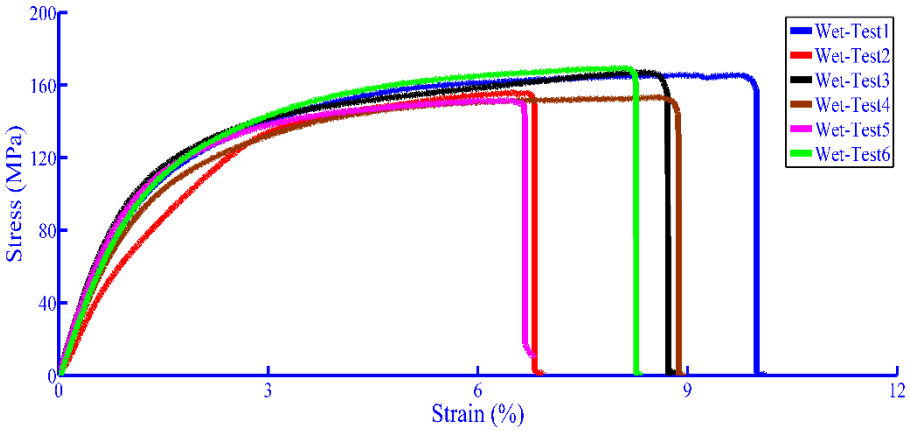

Figure 15. Wet tests for ±45^{o} orientation at room temperature

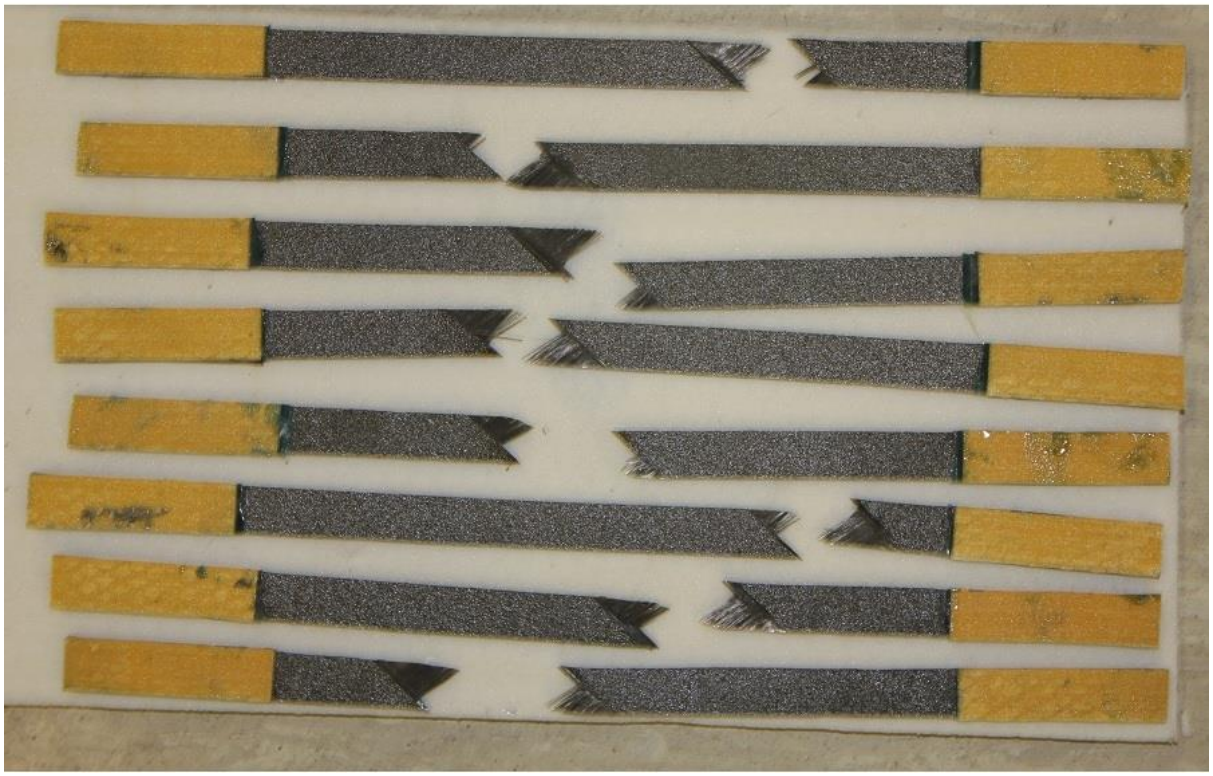

Figure16. Failure surfaces of ±45^{o} orientation specimens for dry test at room temperature

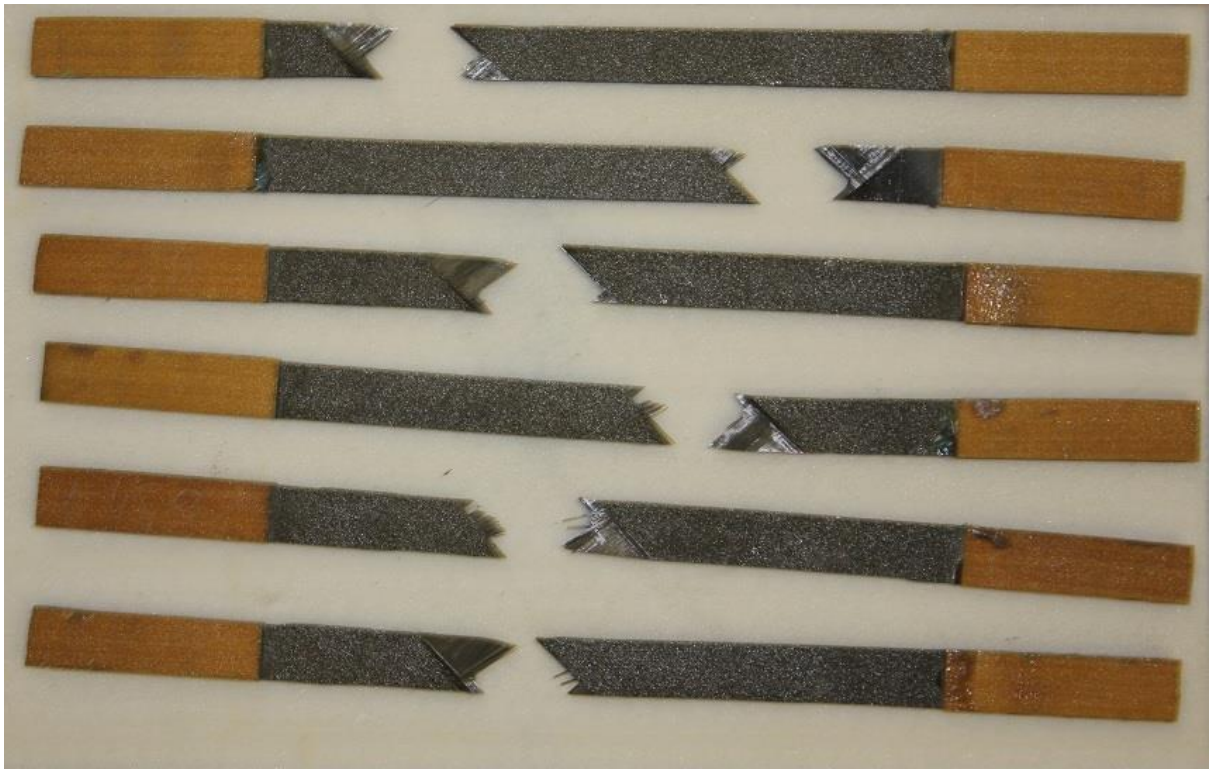

Figure17. Failure surfaces of ±45^{o} orientation specimens for wet test at room temperature

Table 7. Summary of dry test data for *±45^{o}* and Room Temperature

Fracture Load ***kN***	**Strength** ***MPa (ksi)***	**Mean** ***MPa(ksi)***	**Modulus** ***GPa (Msi)***	**Mean** ***GPa (Msi)***
5.52	183.84(26.66)	179.26(26)	8.77(1.27)	8.94(1.30)
5.42	180.58(26.19)		8.55(1.24)	
5.40	179.98(26.1)		9.01(1.31)	
5.41	180.21(26.14)		8.82(1.28)	
5.51	183.62(26.63)		8.71(1.26)	
5.18	172.68(25.04)		9.10(1.32)	
5.30	176(25.63)		9.29(1.34)	
5.29	176(25.59)		9.30(1.35)	

Table 8. Summary of wet test data for ±45^o and Room Temperature

Fracture Load *kN*	Strength *MPa (ksi)*	Mean *MPa(ksi)*	Modulus *GPa (Msi)*	Mean *GPa (Msi)*
4.98	165.97(24.07)	160.75(23.23)	8.75(1.27)	8.63(1.25)
4.68	156.04(22.63)		6.02(0.87)	
5.02	167.36(24.27)		9.56(1.39)	
4.61	153.66(22.29)		8.23(1.19)	
4.55	151.80(22.02)		10(1.45)	
5.09	169.09(24.68)		9.20(1.33)	

1.2.6 Room Temperature Tests at *90^o* Orientation

Dry and wet (moist) specimens were used for room temperature tests for *90^o* orientation. Figures 18 and 19 show the load versus displacement plots for dry and wet specimens at *90^o* orientation. The failed specimens are shown in Figures 20 and 21 respectively. Results for the dry and wet conditions are also summarised in Table 9 and 10, respectively.

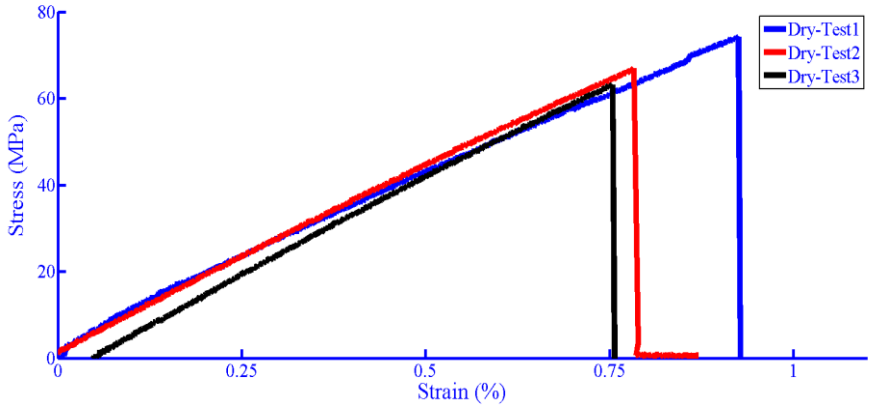

Figure 18. Dry tests for 90^o orientation at room temperature

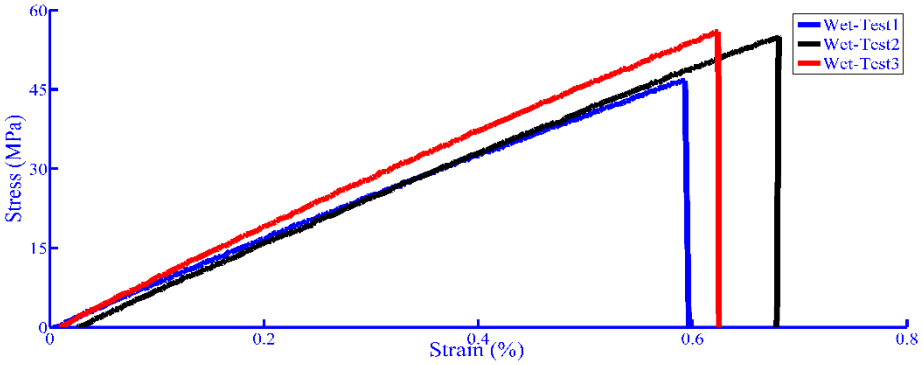

Figure 19. Wet tests for 90^{o} orientation at room temperature

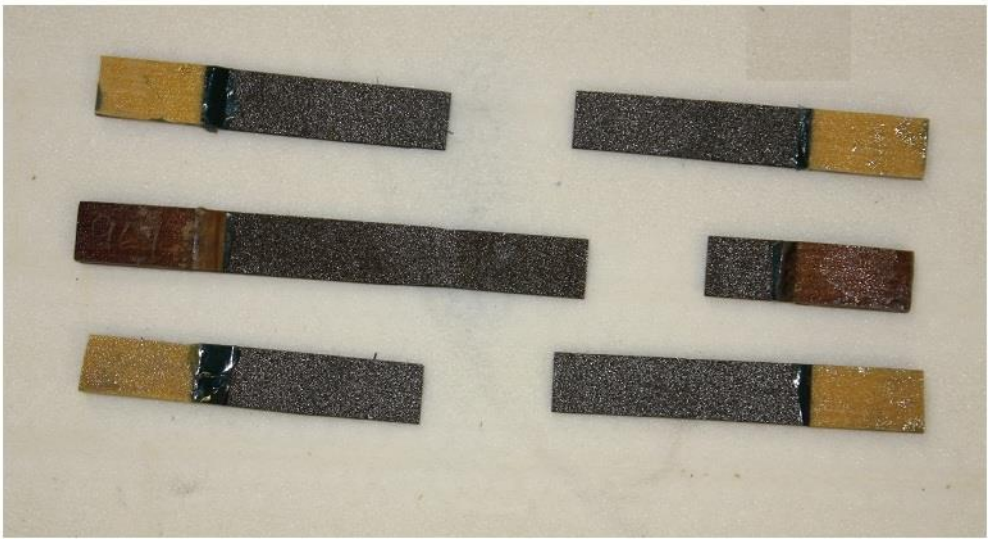

Figure20. Failure surfaces of 90^{o} orientation specimens for dry test at room temperature

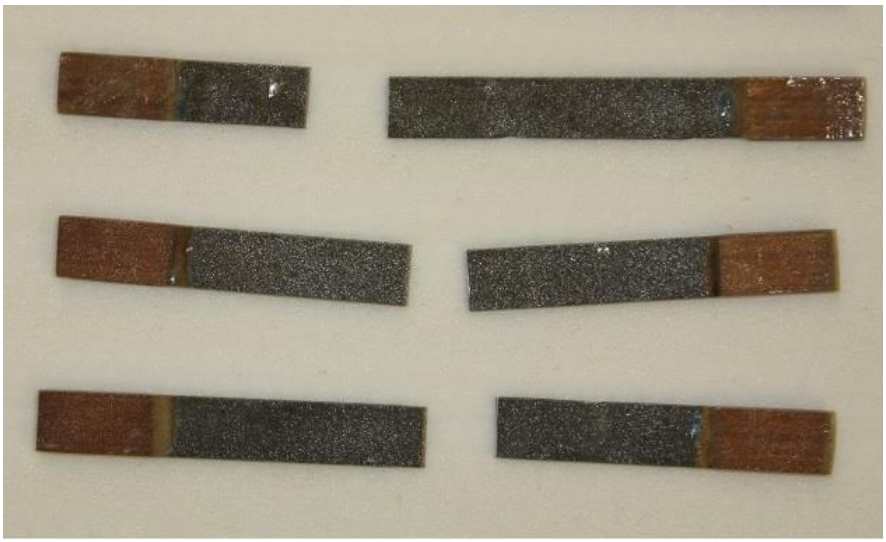

Figure 21. Failure surfaces of 90^{o} orientation specimens for wet test at room temperature

Table 9. Summary of dry test data for 90^o and Room Temperature

Fracture Load ***kN***	**Strength** ***MPa (ksi)***	**Mean** ***MPa(ksi)***	**Modulus** ***GPa (Msi)***	**Mean** ***GPa (Msi)***
2.22	74.16(10.76)	68.11(9.88)	8.00(1.16)	8.30(1.20)
2.01	66.96(9.71)		8.56(1.24)	
1.90	63.20(9.17)		8.35(1.21)	

Table 9. Summary of wet test data for 90^o and Room Temperature

Fracture Load ***kN***	**Strength** ***MPa (ksi)***	**Mean** ***MPa(ksi)***	**Modulus** ***GPa (Msi)***	**Mean** ***GPa (Msi)***
1.4	46.71(6.77)	52.53(7.62)	7.88(1.14)	8.35(1.21)
1.65	54.97(7.97)		8.06(1.17)	
1.68	55.92(8.11)		9.11(1.32)	

1.2.7 Mechanical Testing at High Temperature (*80 °C*)

Specimens were mounted in the grips of the fixture shown in Figure 22. The reason for choosing different a fixture and machine was because these allowed fitting an high temperature environmental chamber into the test setup. The specimens were mounted in the fixture and a metallic bar was used to connect the fixture with load cell. This way, the load cell is protected from exposure to a temperature above its operating range. The chamber used for the tests is well capable of maintaining the gauge section of the coupons at the required temperature. All the specimens (Dry and Wet) considered for high temperature testing (80 °C) were characterised using the same machine and environmental chamber shown in Figure 23. The clamping opressure on the end tab of the specimens was manually adjusted until both slippage and failure close to the tabs were avoided. Extra care is needed to mount the specimen in the fixture, especially for the case of 90^o coupons. Apart from pressure, all other test specification were kept same as reported in the section 4.1.

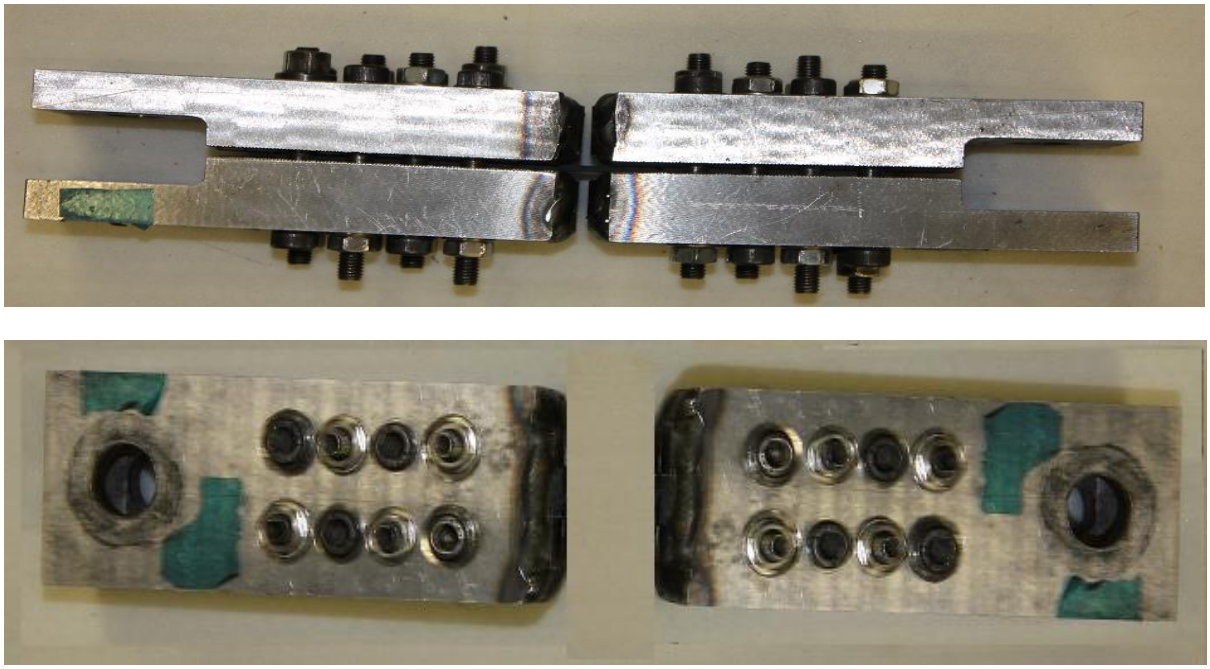

Figure 22. Fixture used for mechanical testing at high temperature (Top and side view)

Figure 23. Mechanical testing setup for high temperature (Front and side view of the chamber)

1.2.8 High Temperature (*80 °C)* Tests at 0^o Orientation

Dry and wet (moist) specimens with 0^o orientation were tested at high temperature. Figures 24 and 25 show the load versus displacement plots for dry and wet specimens with 0^o orientation, tested at *80 °C.* The failed specimens are shown in Figures 26 and 27 respectively. Results for the dry and wet conditions are summarised in Table 11 and 12 respectively.

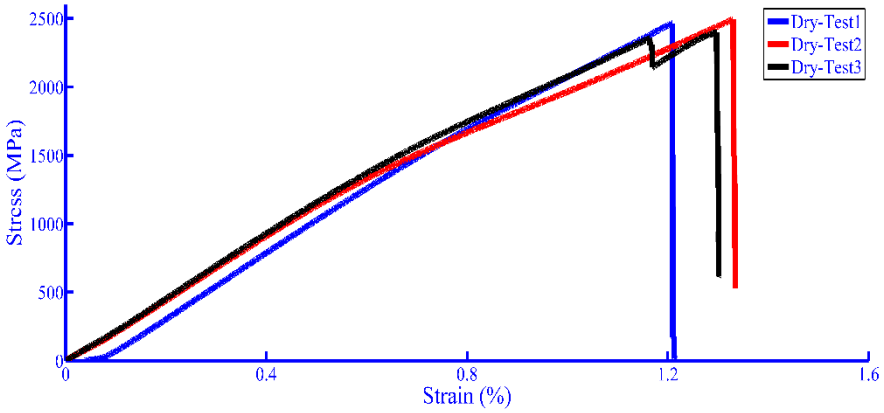

Figure 24. Dry tests for 0^o orientation at 80 °C

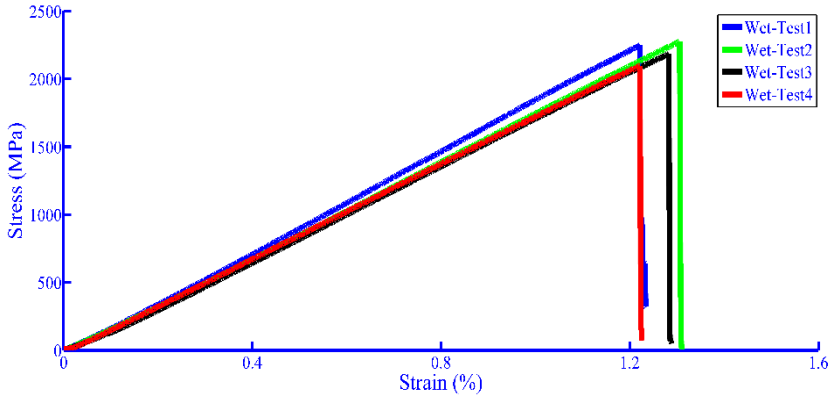

Figure 25. Wet tests for 0^o orientation at *80* °C

Figure26. Failure surfaces of 0^o orientation specimens for dry test at 80 °C

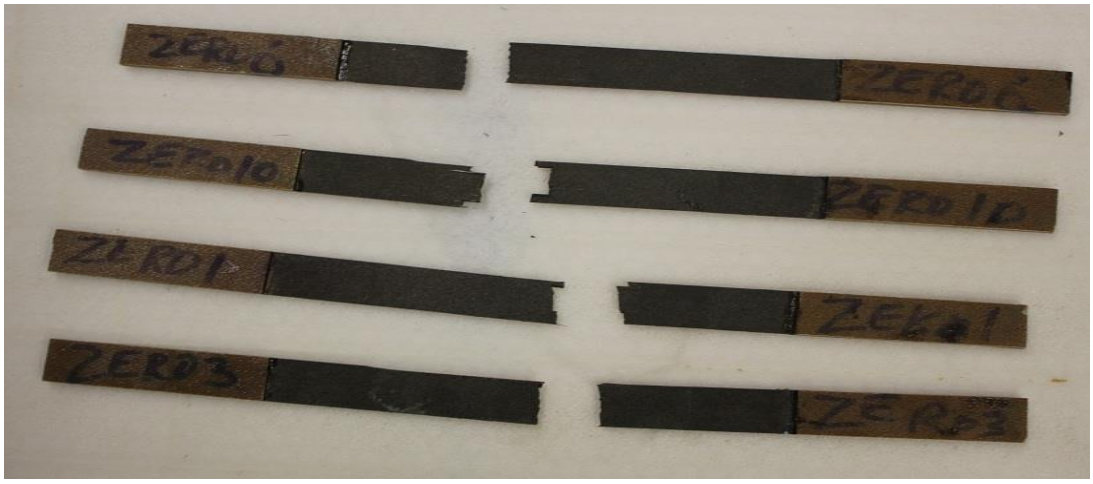

Figure27. Failure surfaces of 0^o orientation specimens for wet tests at 80 °C

Table 11. Summary of dry test data for 0^o at 80 °C

Fracture Load ***kN***	**Strength** ***MPa (ksi)***	**Mean** ***MPa(ksi)***	**Modulus** ***GPa (Msi)***	**Mean** ***GPa (Msi)***
30.30	2463.24(357.26)	2453.33(355.50)	188.16 (27.29)	186.67 (27.07)
30.66	2492.84(361.56)		174.51(25.31)	
29.49	2397.25(347.69)		197.32 (28.62)	

Table 12. Summary of wet test data for 0^o at 80 °C

Fracture Load ***kN***	**Strength** ***MPa (ksi)***	**Mean** ***MPa(ksi)***	**Modulus** ***GPa (Msi)***	**Mean** ***GPa (Msi)***
27.66	2249.14(326.21)	2201.89(319.36)	184.22 (23.77)	175.10(25.4)
28.01	2276.63(330.20)		174.35 (22.53)	
26.86	2183.41(316.68)		170.13 (21.97)	
25.81	2098.37(304.34)		171.69 (22.16)	

1.2.9 High Temperature (*80 °C*) Tests at ±*45*^{o} Orientation

Dry and wet (moist) specimens with ±*45*^{o} orientation were considered for high temperature tests. Figures 28 and 29 show the load-displacement plots for dry and wet specimens with ±*45*^{o} orientation at *80 °C*, while Figures 30 and 31 show the failed specimens, respectively. Results for the dry and wet conditions are summarised in Table 13 and 14.

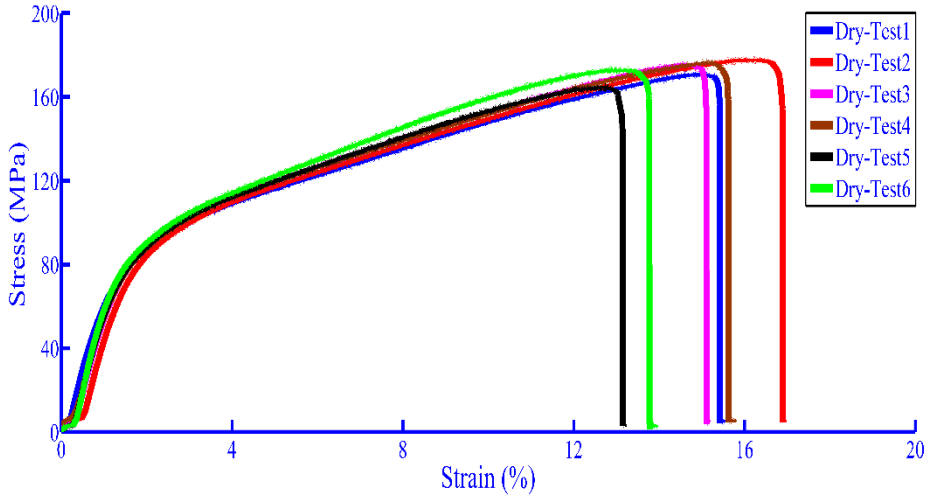

Figure 28. Dry tests for ±45^{o} orientation at 80 °C

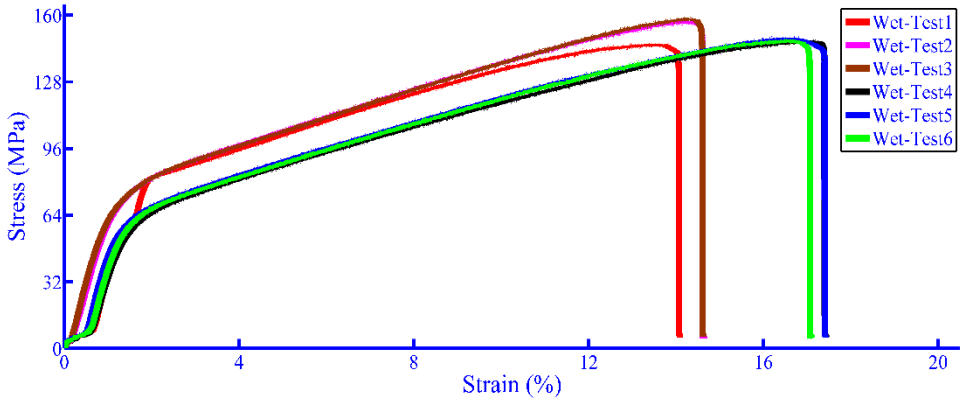

Figure 29. Wet tests for ±45^{o} orientation at 80 °C

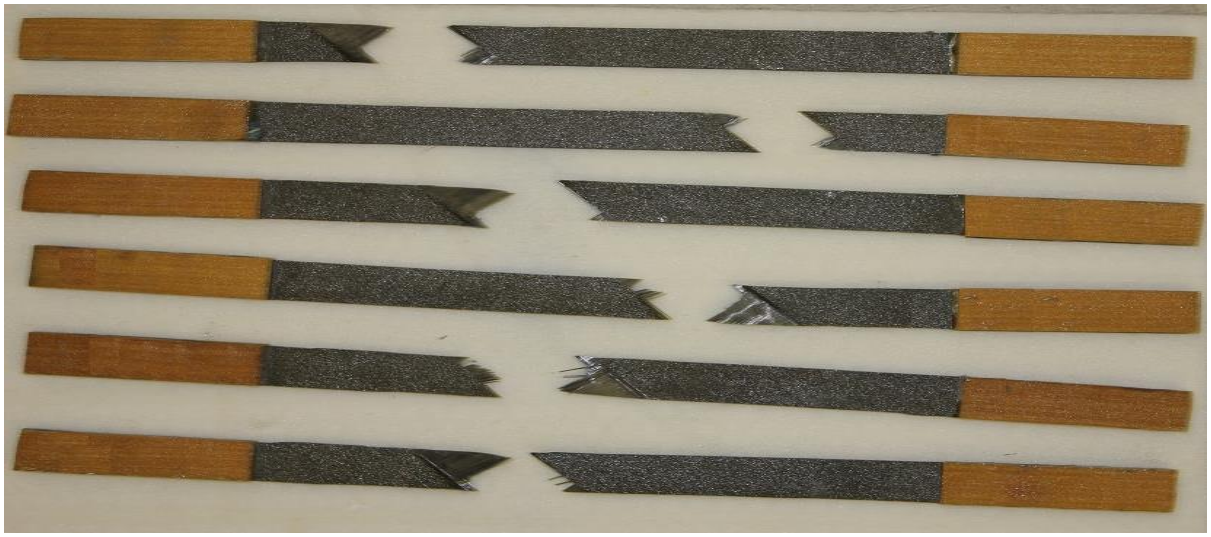

Figure 30. Failure surfaces of ±45^{o} orientation specimens for dry tests at 80 °C

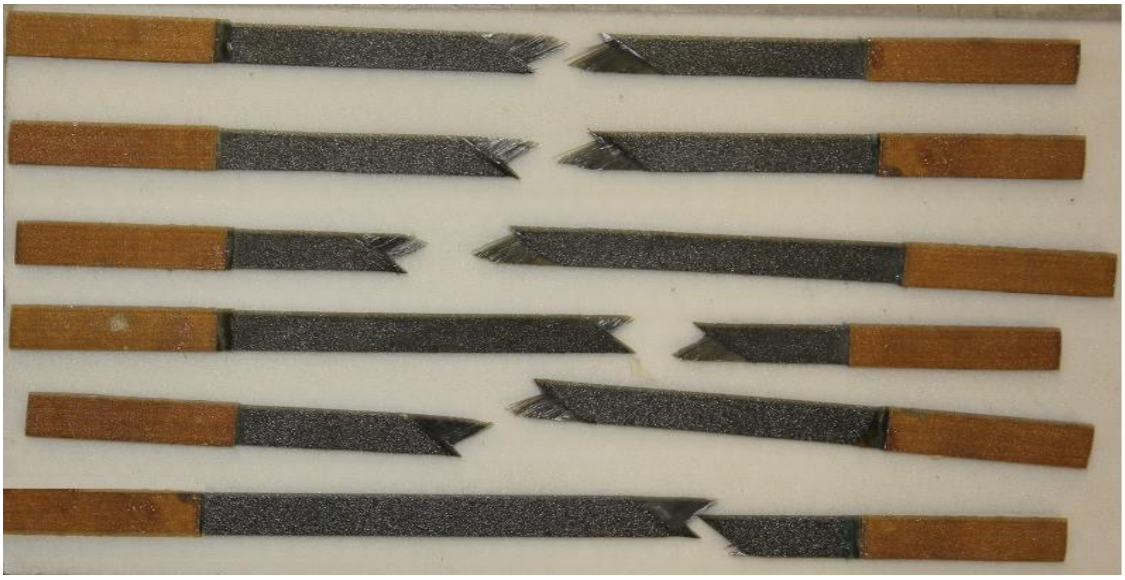

Figure 31. Failure surfaces of ±45^{o} orientation specimens for wet test at 80 °C

Table 13. Summary of dry tests data for ±45^{o} at 80 °C

Fracture Load *kN*	**Strength** *MPa (ksi)*	**Mean** *MPa(ksi)*	**Modulus** *GPa (Msi)*	**Mean** *GPa (Msi)*
5.14	171.26(24.84)	173.31(25.14)	5.59(0.81)	5.32(0.77)
5.34	178.14(25.84)		4.61(0.67)	
5.28	176.01(25.53)		5.24(0.76)	

5.30	176.55(25.61)		5.34(0.77)	
4.94	164.80(23.90)		5.43(0.79)	
5.19	173.11(25.11)		5.68(0.82)	

Table 14. Summary of wet tests data for ±45^o at 80 °C

Fracture Load ***kN***	**Strength** ***MPa (ksi)***	**Mean** ***MPa(ksi)***	**Modulus** ***GPa (Msi)***	**Mean** ***GPa (Msi)***
4.39	146.18(21.20)	151.10(21.92)	3.85(0.56)	4.01(0.58)
4.71	157.13(22.79)		4.39(0.64)	
4.75	158.42(22.98)		3.49(0.51)	
4.43	147.68(21.42)		3.81(0.55)	
4.47	149.09(21.62)		4.46(0.65)	
4.44	148.12(21.48)		4.08(0.59)	

1.2.10 High Temperature (*80 °C*) Tests at *90^o* Orientation

Dry and wet (moist) specimens were used for high temperature tests for *90^o* orientation. Figures 33 and 34 show the plots for dry and wet specimens at *90^o* orientation at *80 °C* while the corresponding failure in the specimens is shown in Figures 35 and 36 respectively. For these coupons, the load introduction proved difficult, due to the sliding of the rod for the attachment to the load cell. This did not happen for the room temperature testing, when the specimens were mounted directly in the grips of the machine. Results for the dry and wet conditions are also summarised in Table 15 and 16 respectively.

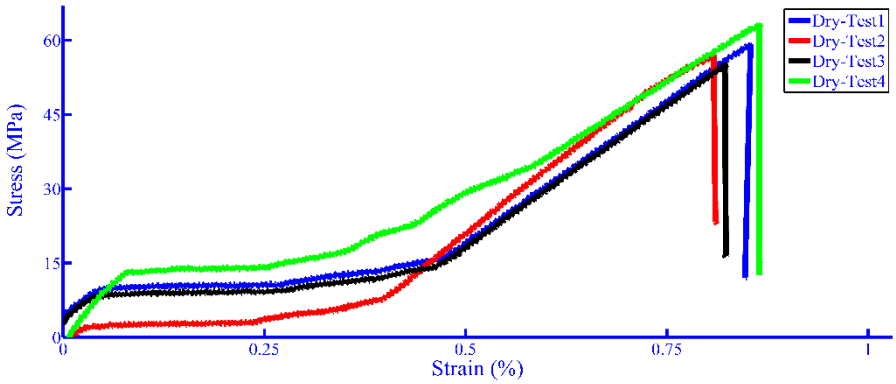

Figure 32. Dry tests for 90^o orientation at 80 °C

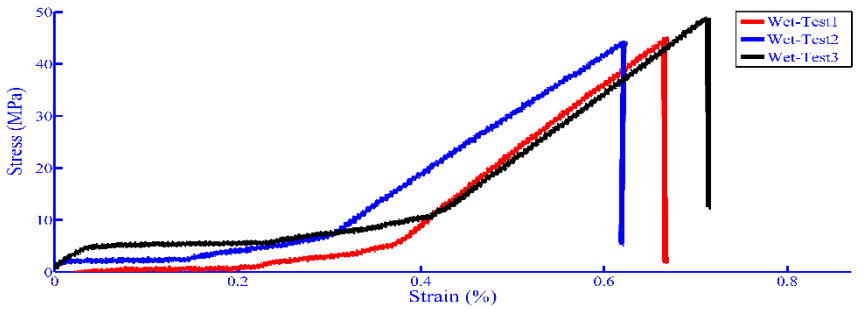

Figure 33. Wet tests for 90^{o} orientation at 80 °C

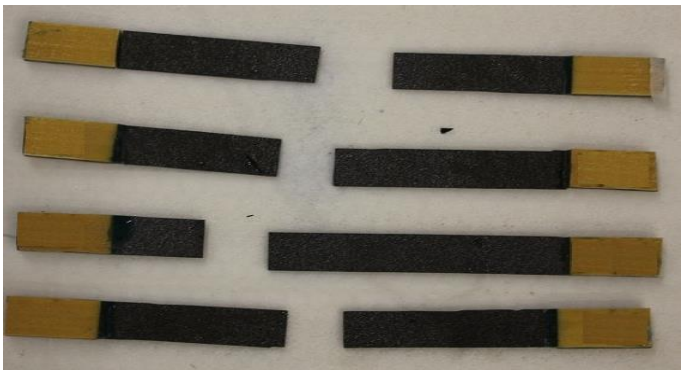

Figure 34. Failure surfaces of 90^{o} orientation specimens for dry test at 80 °C

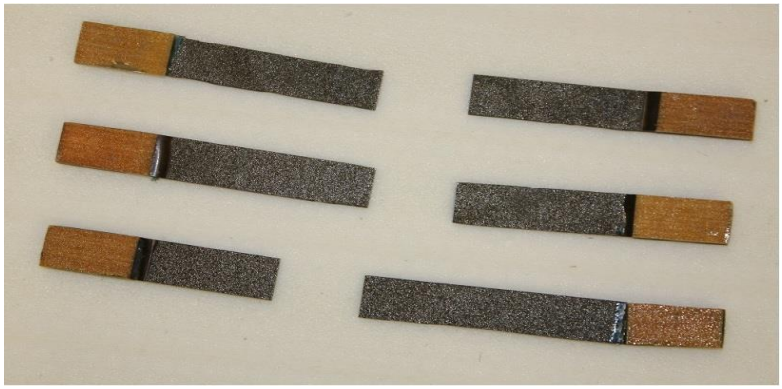

Figure 35. Failure surfaces of 90^{o} orientation specimens for wet test at 80 °C

Table 15. Summary of dry tests data for 90^{o} at 80 °C

Fracture Load *kN*	**Strength** *MPa (ksi)*	**Mean** *MPa(ksi)*	**Modulus** *GPa (Msi)*	**Mean** *GPa (Msi)*
1.78	59.23(8.59)	52.53(8.52)	6.93(1.01)	6.99(1.01)
1.71	56.99(8.27)		7.05(1.02)	
1.66	55.38(8.03)		6.70(0.97)	

1.90	63.45(9.20)		7.29(1.06)	

Table 16. Summary of wet tests data for 90^o at 80 °C

Fracture Load ***kN***	**Strength** ***MPa (ksi)***	**Mean** ***MPa(ksi)***	**Modulus** ***GPa (Msi)***	**Mean** ***GPa (Msi)***
1.35	45.16(6.55)	46.13(6.70)	6.70(0.97)	6.90(1.00)
1.33	44.41(6.44)		7.14(1.04)	
1.46	48.83(7.08)		6.84(0.99)	

1.3 Compression Testing

1.3.1 Manufacturing of Specimens

The specimen used for compression testing was same i.e. IM7 12k/977-2 as was used for the tensile testing.

The lay-up angles, 0^o, $\pm45^o$ and 90^o, reported refer to the orientation of the longitudinal fibre direction. After manually laying up the $[0]_{10}$, $[\pm45]_{16}$ and $[90]_{16}$ layups, the plies were cured in autoclave. A milling cutter was used to cut the laminate panels into the required coupons sizes. The specimen dimensions used for the mechanical testing are summarised in table 17 and are also shown in Figures 36-38. To improve the joints strength, grit blasting was performed to prepare the surfaces for the Letoxit LH 149 was used for bonding the tabs to the coupon. The bond-line thickness was found again to be in the range 0.1-0.2 *mm*. The bonded parts were cured for 4 hours at 50 *°C* in oven.

Table 17. Composite Specimen Geometry

Fibre Orientation	**Width (*mm*)**	**Overall Length (*mm*)**	**Gauge Length (*mm*)**	**Thickness (*mm*)**	**Tab Length (*mm*)**	**Tab Thickness (*mm*)**	**Tab Bevel Angle**
0^o	9.75	90	10	2	40	2	90
$\pm45^o$	9.75	90	10	3.2	40	2	90
90^o	9.75	90	10	3.2	40	2	90

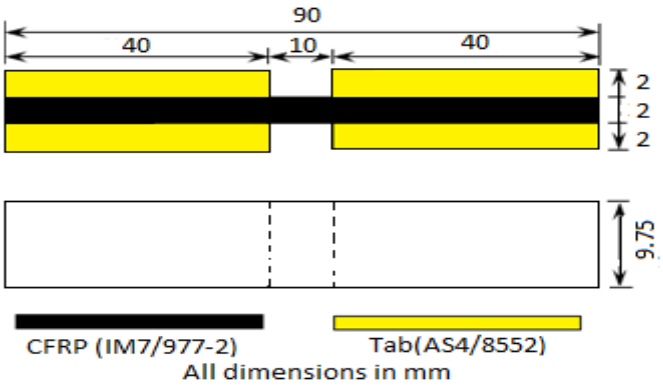

Figure 36. Typical specimen used for 0^o unidirectional layup

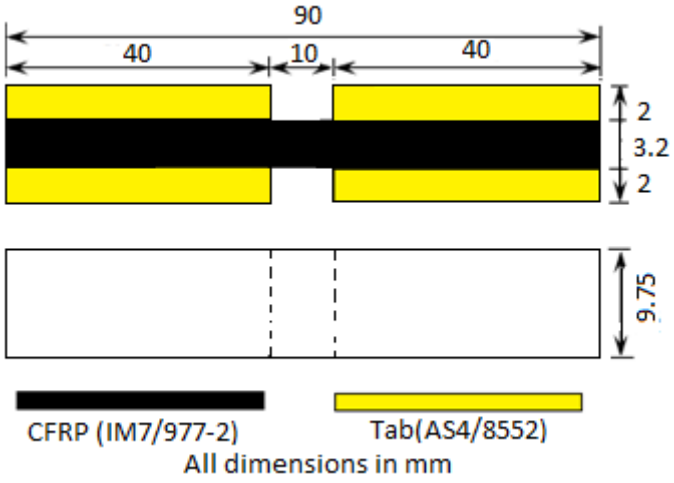

Figure 37. Typical specimen used for $\pm 45^o$ unidirectional layup

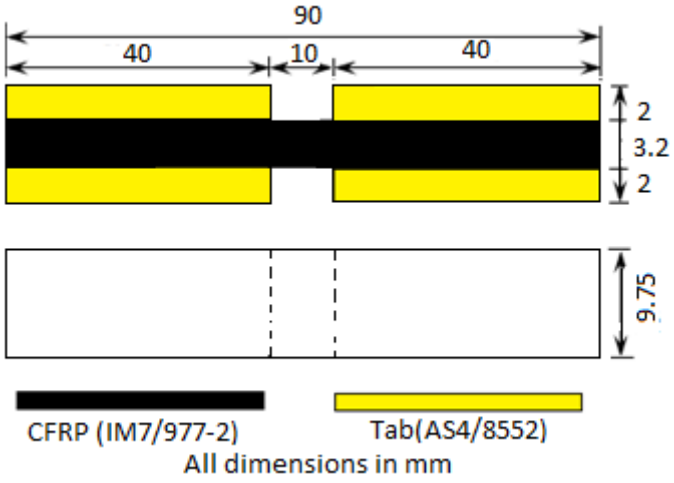

Figure 38. Typical specimen used for 90^o unidirectional layup

1.3.2 Humidity Conditioning

The moisture ingress in the specimens was carried out in the same water bath used for the tensile coupons, shown in Figure 39. Again the temperature of the water bath was raised to 80 *°C* in order to accelerate the moisture uptake. The humidity conditioning was performed on 9 specimens with 0^o orientation, 11 (1 specimen failed during the testing setting-up) specimens with $\pm 45^o$ orientation and 9 (2 out of 9 broke during the setting up in compression testing jig shown later in the report) with 90^o layup. The $\pm 45^o$ and 90^o coupons were placed in the water bath on 8th May, 2014 and were tested between 4th and 15th August, 2014. For the 0^o coupons, the thickness of the specimens was reduced to 2 *mm* and a release film of 15 *mm* length and 9.75 *mm* was inserted between the CFRP and end tab. This brought the failure load to levels similar to those quoted in the literature. However, the failure mode involved delaminations emanating from the tab regions. To avoid this problem, specimens with 0^o orientation were manufactured without the release film. On 1st August, 2014, the 0^o layup specimens were placed in the water bath and the water bath temperature was kept at *80°C* to proceed with a faster conditioning. The weight gain of the compression coupons was monitored daily, as already done for the tensile specimens.

Figure 39. Water bath to moisture the specimens

Table 18. Moisture gain for 0^o orientation specimens

Fibre Orientation	Dry Specimen Weight(*gms*)	Weight before Testing (*gms*)	Moisture Contents (*gms*)	Moisture contents (*%*)
0^o	6.0281	6.1087	0.0806	1.34
0^o	6.0671	6.1424	0.0753	1.24

0^o	6.1072	6.1797	0.0725	1.19
0^o	6.0762	6.1534	0.0772	1.27
0^o	6.0798	6.1591	0.0793	1.30
0^o	6.0733	6.1505	0.0772	1.27
0^o	5.9813	6.0718	0.0905	1.51

Table 19. Moisture gain for ±45^o orientation specimens

Fibre Orientation	**Dry Specimen Weight(*gms)***	**Weight before Testing (*gms*)**	**Moisture Contents (*gms*)**	**Moisture contents (*%)***
±45^o	9.1773	9.2979	0.1206	1.31
±45^o	9.0663	9.1703	0.104	1.15
±45^o	8.7818	8.8931	0.1113	1.27
±45^o	9.1066	9.2212	0.1146	1.26
±45^o	8.9403	9.0534	0.1131	1.27
±45^o	9.0213	9.1231	0.1018	1.13
±45^o	7.9948	8.1301	0.1353	1.69
±45^o	8.2808	8.4182	0.1374	1.66
±45^o	8.1097	8.2507	0.141	1.74
±45^o	8.829	8.9268	0.0978	1.11
±45^o	8.1043	8.2165	0.1122	1.38

Table 20. Moisture gain for 90^o orientation specimens

Fibre Orientation	Dry Specimen Weight*(gms)*	Weight before Testing (*gms*)	Moisture Contents (*gms)*	Moisture contents (*%)*
90^o	8.8199	8.9512	0.1313	1.49
90^o	8.8242	8.9615	0.1373	1.56
90^o	8.8592	8.9729	0.1137	1.28
90^o	8.9394	9.0421	0.167	1.15
90^o	9.0569	9.1554	0.0985	1.09
90^o	8.9566	9.0718	0.1152	1.29
90^o	8.7994	8.899	0.0996	1.13
90^o	8.7696	8.8766	0.107	1.22
90^o	8.9029	9.0256	0.1227	1.38

1.3.3 Compression Testing at Room Temperature

A Zwick 1478 servo-hydraulic machine with 100 *kN* load capacity was used for specimens testing at room temperature, as shown in Figure 40. The tests were performed at a rate of 1 *mm/min*. The tests were repeated for a minimum of 3 times for the each set of environmental conditions. The specimens were placed in the compression jig shown in Figure 41. The tests confirmed that the compressive failure occurred within the specimen gauge section.

Figure 40. Machine used for the specimens testing at room temperature

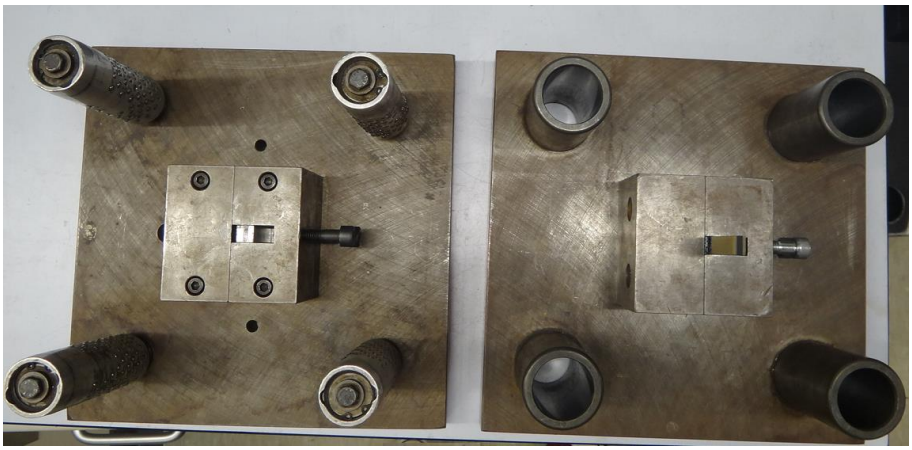

Figure 41 Compression jig used for mechanical testing (Top and side view)

1.3.4 Room Temperature Tests at 0^o Orientation

Dry and wet (moist) specimens were considered in room temperature tests for the 0^o orientation. Figures 42and 43 show the plots for dry and wet specimens at 0^o orientation, while the corresponding failure mode in the specimens is shown in Figures 44 and 45 respectively.. Results for the dry and wet conditions are summarised in Table 21.

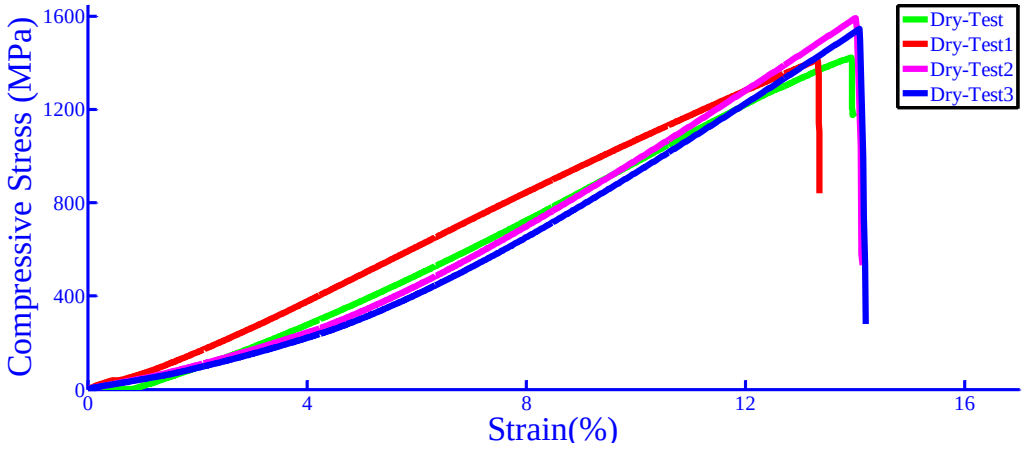

Figure 42. Dry tests for 0^o orientation at room temperature

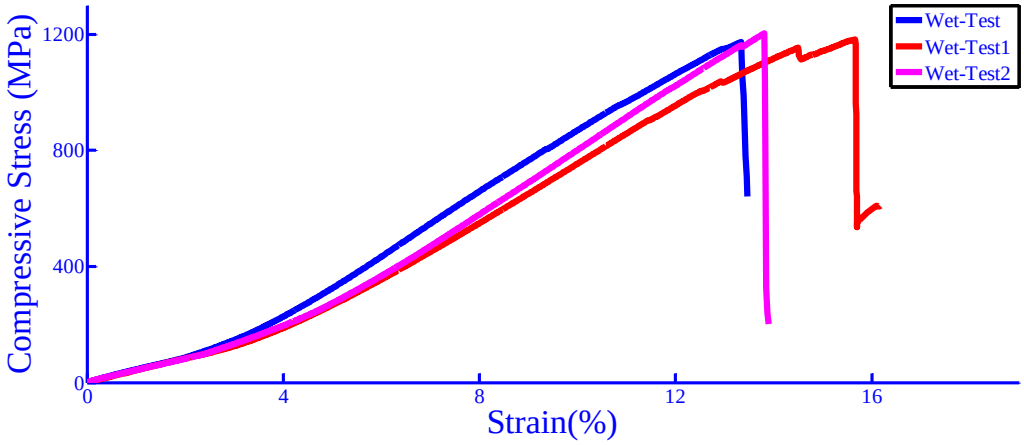

Figure 43. Wet tests for 0^o orientation at room temperature

Figure 44. Failure surfaces of 0^o orientation specimens for dry test at room temperature

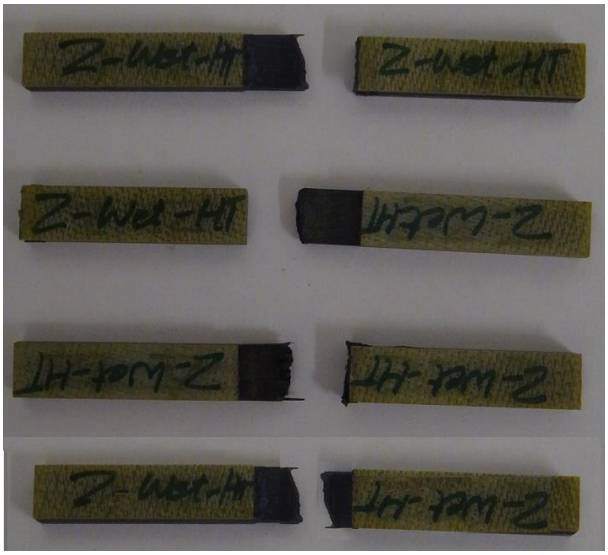

Figure 45. Failure surfaces of 0^o orientation specimens for wet test at room temperature

Table 21. Summary of test data for 0^o orientation at room temperature

Test condition	Compressive fracture load *kN*	Compressive strength *MPa (ksi)*	Mean *MPa(ksi)*
Dry	27.75	1423.6(206.47)	1494(216.68)
Dry	27.57	1414.2(205.11)	
Dry	31.05	1592.4(230.96)	
Dry	30.14	1545.7(224.18)	
Wet	22.88	1173.4(170.13)	1186.9(172.14)
Wet	23.06	1183(171.57)	
Wet	23.48	1204.2(174.66)	

1.3.5 Room Temperature Tests at $\pm 45^o$ Orientation

Dry and wet (moist) specimen were considered for the room temperature tests for the $\pm 45^o$ orientation. Figures 46 and 47 show the plots for dry and wet specimens at $\pm 45^o$ orientation, while the corresponding failure mode in each specimen is shown in Figures 48 and 49, respectively. Results for the dry and wet conditions are also summarised in Table 22.

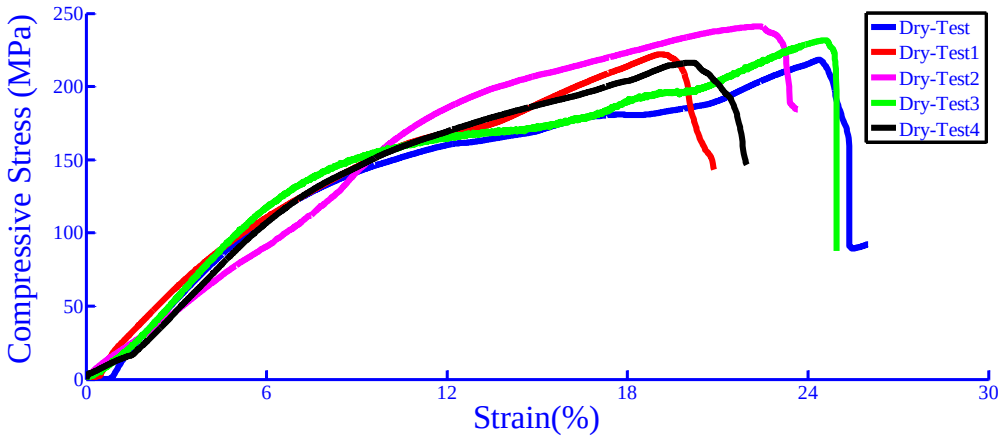

Figure 46. Dry tests for ±45^{o} orientation at room temperature

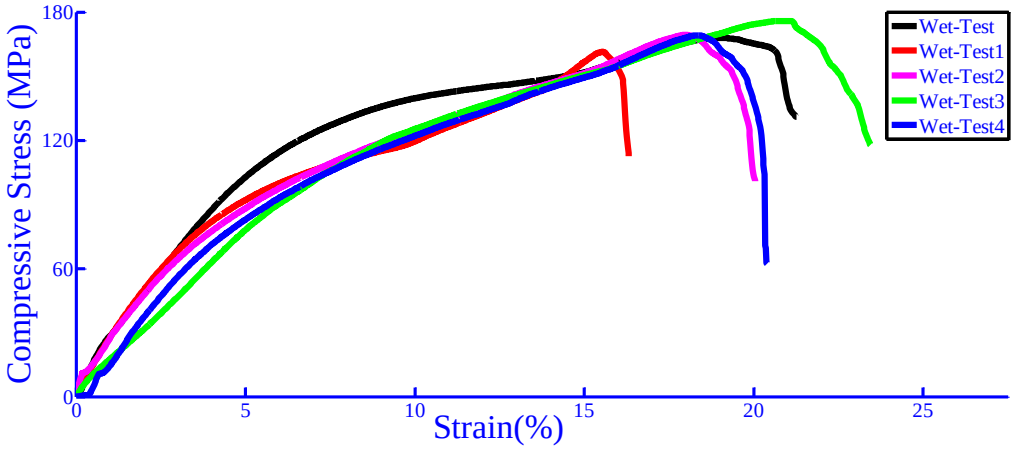

Figure 47. Wet tests for ±45^{o} orientation at room temperature

Figure 48. Failure surfaces of ±45^{o} orientation specimens for dry test at room temperature

Figure 49. Failure surfaces of ±45^{o} orientation specimens for wet test at room temperature

Table 22. Summary of test data for ±45^{o} at room temperature

Test condition	**Compressive fracture load** *kN*	**Compressive strength** *MPa (ksi)*	**Mean** *MPa(ksi)*
Dry	6.81	218.35(31.65)	225.86(32.76)
Dry	6.93	222.13(32.22)	
Dry	7.52	241.04(34.96)	
Dry	7.23	231.63(33.60)	
Dry	6.75	216.25(31.36)	
Wet	5.24	167.81(24.33)	
Wet	5.03	161.29(23.39)	

Wet	5.28	169.26(24.54)	168.67(24.46)
Wet	5.49	175.90(25.51)	
Wet	5.28	169.08(24.52)	

1.3.6 Room Temperature Tests at 90^o Orientation

Dry and wet (moist) specimens were used for room temperature tests for 90^o orientation. Figures 50 and 51 show the plots for dry and wet specimens at 90^o orientation while the corresponding failure in the specimens is shown in Figures 52 and 53 respectively. Results for the dry and wet conditions are also summarised in Table 23.

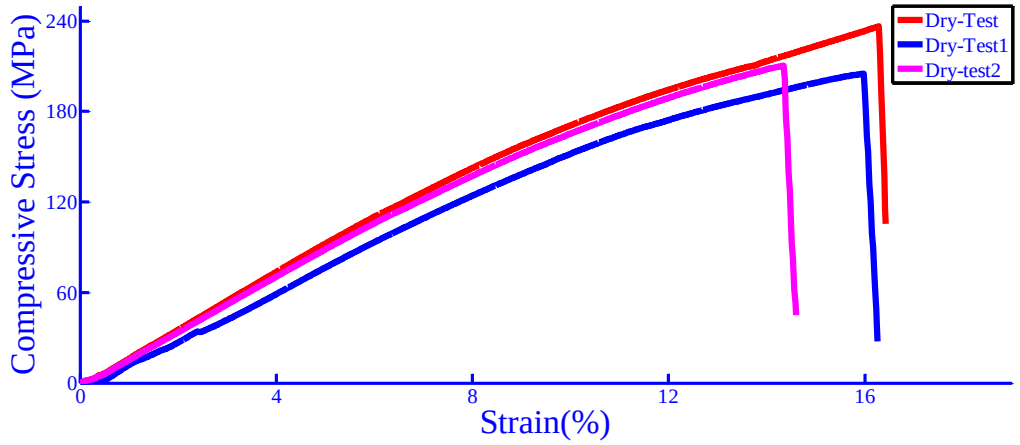

Figure 50. Dry tests for 90^o orientation at room temperature

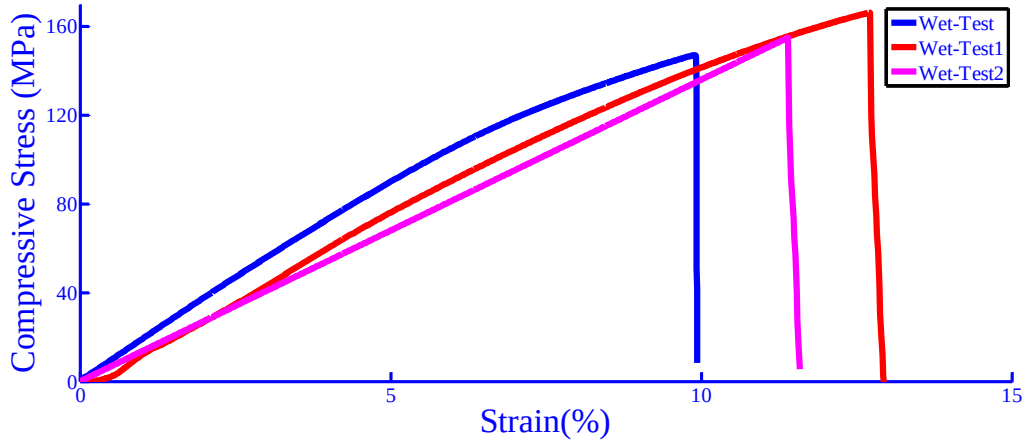

Figure 51. Wet tests for 90^o orientation at room temperature

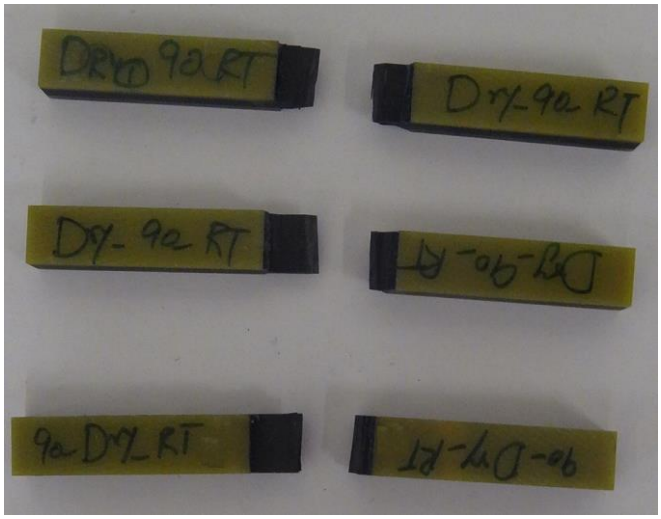

Figure 52. Failure surfaces of 90^{o} orientation specimens for dry test at room temperature

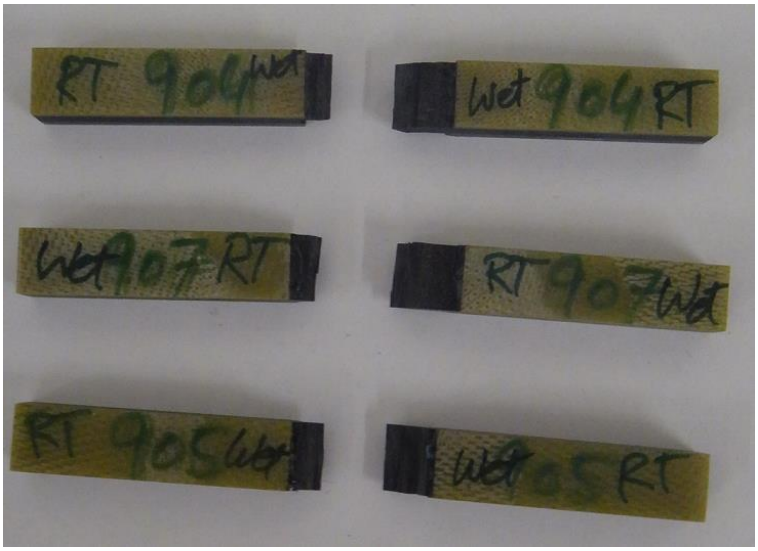

Figure 53. Failure surfaces of 90^{o} orientation specimens for wet test at room temperature

Table 23. Summary of test data for 90^{o} orientation at room temperature

Test condition	**Compressive fracture load** ***kN***	**Compressive strength** ***MPa (ksi)***	**Mean** ***MPa(ksi)***
Dry	7.37	236.37(34.28)	217.21(31.50)
Dry	6.39	204.90(29.72)	
Dry	6.56	210.35(30.51)	
Wet	4.59	146.96(21.31)	

Wet	5.19	166.21(24.11)	156.07(22.64)
Wet	4.84	155.05(22.49)	

1.3.7 Compression Testing at High Temperature (*80 °C*)

Specimens were mounted in the grips of compression jig as shown in Figure 41. A high temperature environmental chamber was used, as shown in Figure 54 for high temperature testing on the Zwick 1478 machine. The specimens were mounted in the compression jig. The load cell was protected keeping it outside the environmental chamber.

Front view **Side vide**

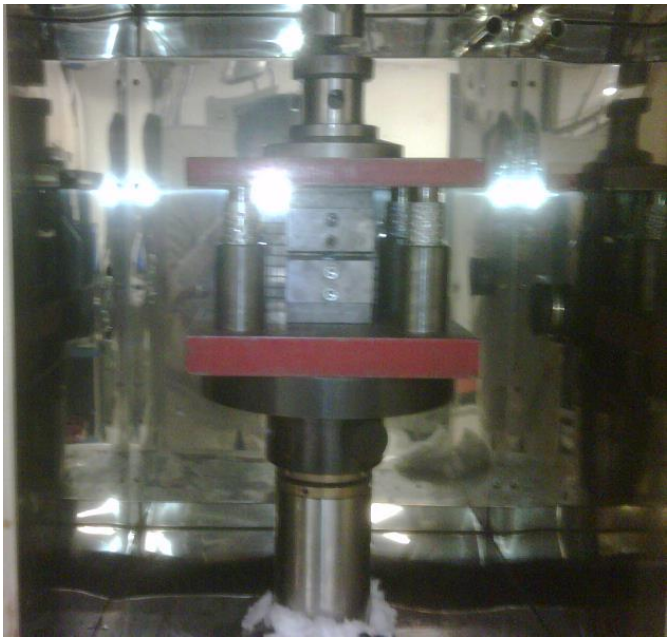

Inside view

Figure 54. Mechanical testing setup for high temperature condition (Front, side and inside view of the chamber)

1.3.8 High Temperature (*80 °C)* Tests at 0^o Orientation

Figures 55 and 56 show the load-displacement plots for dry and wet specimens at 0^o orientation tested at *80 °C*. Figures 57 and 58 show the failure mode for dry and wet specimens, respectively. Results for the dry and wet conditions are summarised in Table 24.

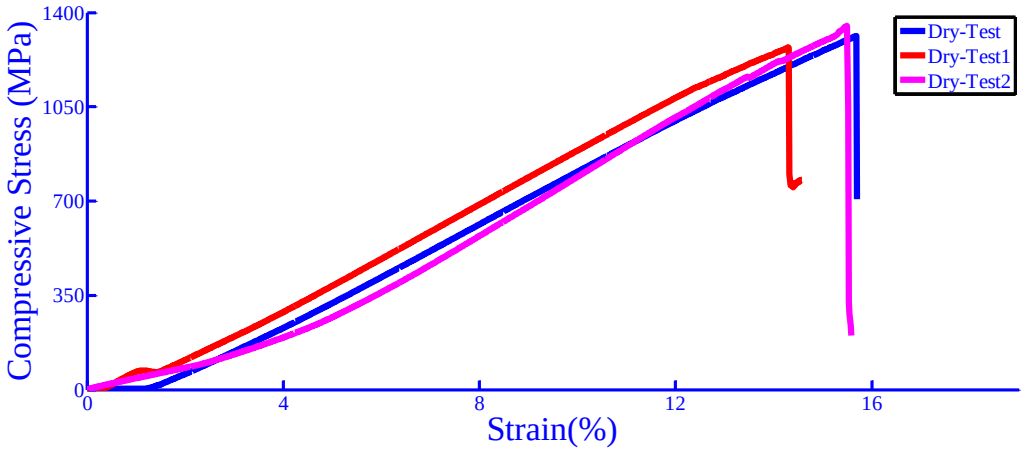

Figure 55. Dry tests for 0^o orientation at 80 °C

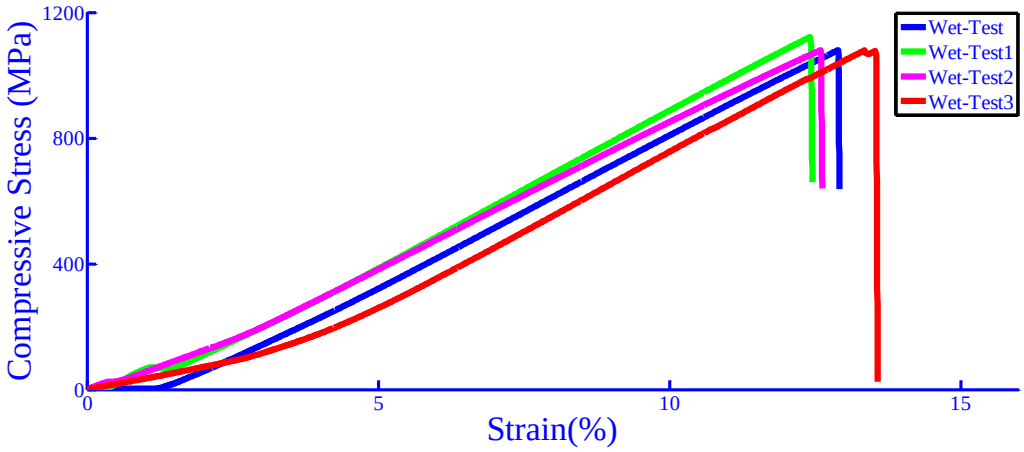

Figure 56. Wet tests for 0^o orientation at *80* °C

Figure 57. Failure surfaces of 0^o orientation specimens for dry test at 80 °C

Figure 58. Failure surfaces of 0^o orientation specimens for wet tests at 80 °C

Table 24. Summary of test data for 0^o orientation at 80 °C

Test condition	Compressive fracture load *kN*	Compressive strength *MPa (ksi)*	Mean *MPa(ksi)*
Dry	25.61	1313.3(190.48)	1311.5(190.21)
Dry	24.77	1270.2(184.22)	
Dry	26.34	1350.9(195.94)	
Wet	21.06	1079.9(156.63)	1090.2(158.13)
Wet	21.88	1122(162.74)	
Wet	21.06	1080.1(156.65)	
Wet	21.04	1078.9(156.48)	

1.3.9 High Temperature (*80 °C*) Tests at $\pm 45^o$ Orientation

Dry and wet (moist) specimens with $\pm 45^o$ orientation were tested at high temperature. Figures 59 and 60 show the load versus displacement plots for dry and wet specimens with $\pm 45^o$ orientation at *80 °C*, while Figures 61 and 62 show the corresponding failure modes. Results for the dry and wet conditions are summarised in Table 25.

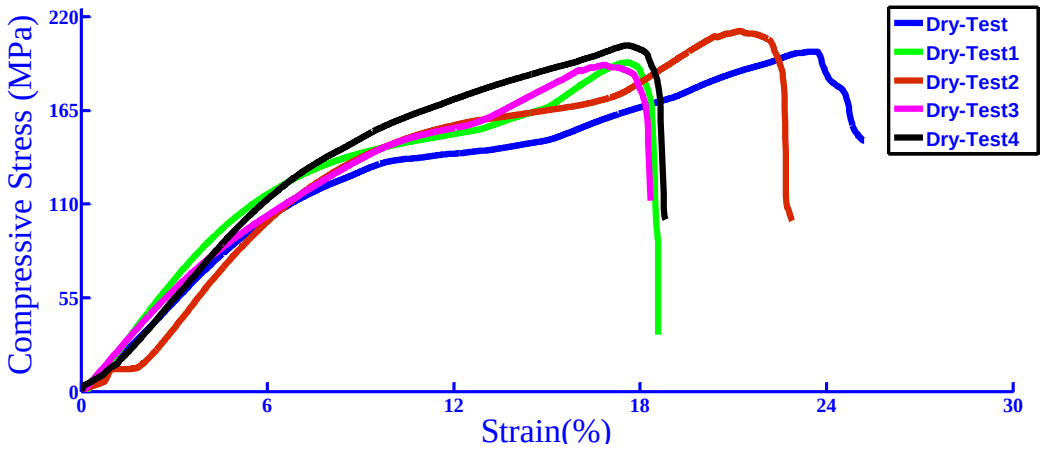

Figure 59. Dry tests for $\pm 45^o$ orientation at 80 °C

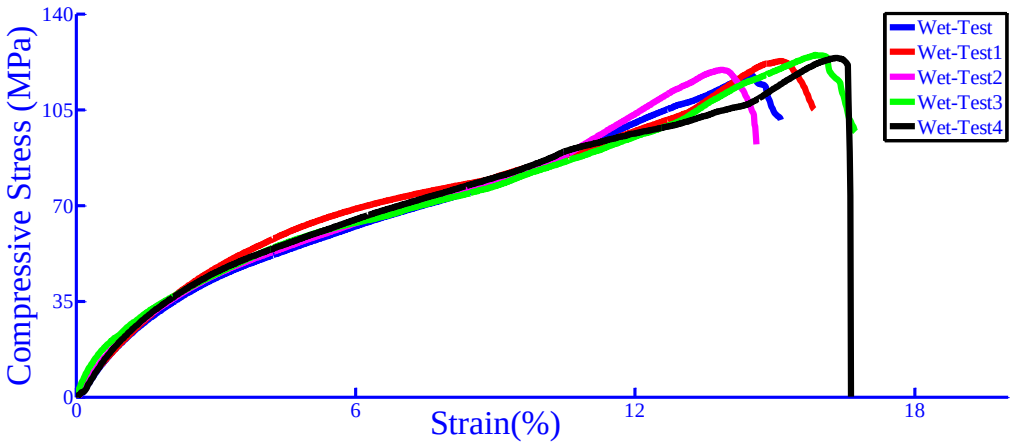

Figure 60. Wet tests for ±45° orientation at 80 °C

Figure 61. Failure surfaces of ±45° orientation specimens for dry test at 80 °C

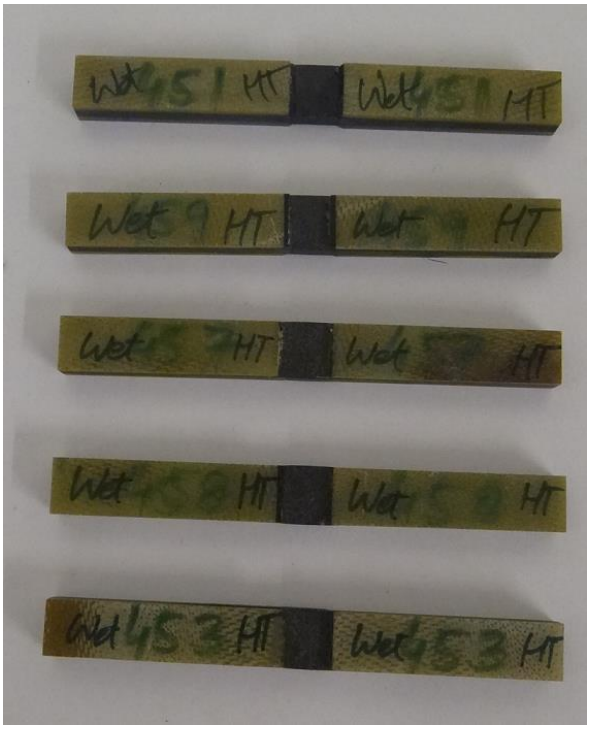

Figure 62. Failure surfaces of ±45^{o} orientation specimens for wet test at 80 °C

Table 25. Summary of test data for ±45^{o} at 80 °C

Test condition	**Compressive fracture load** ***kN***	**Compressive strength** ***MPa (ksi)***	**Mean** ***MPa(ksi)***
Dry	6.22	199.46(28.92)	199.85(28.98)
Dry	6.03	193.28(28.03)	
Dry	6.60	211.67(30.70)	
Dry	5.98	191.79(27.82)	
Dry	6.34	203.07(29.45)	
Wet	3.67	117.55(17.05)	121.70(17.65)
Wet	3.83	122.65(17.79)	
Wet	3.73	119.48(17.33)	
Wet	3.9	124.98(18.13)	
Wet	3.86	123.82(17.96)	

1.3.10 High Temperature (*80 °C*) Tests at 90^o Orientation

Dry and wet (moist) specimens with 90^o orientation were tested at high temperature. Figures 63 and 64 show the load-displacement plots for dry and wet specimens with 90^o orientation, characterised at *80 °C*. The failure modes for the specimens are shown in Figures 65 and 66 respectively. Results for the dry and wet conditions are also summarised in Table 26.

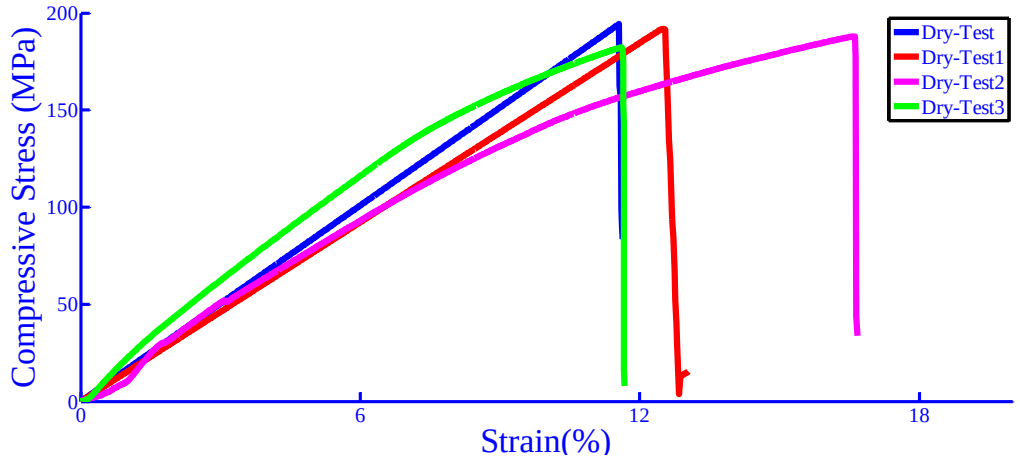

Figure 63. Dry tests for 90^o orientation at 80 °C

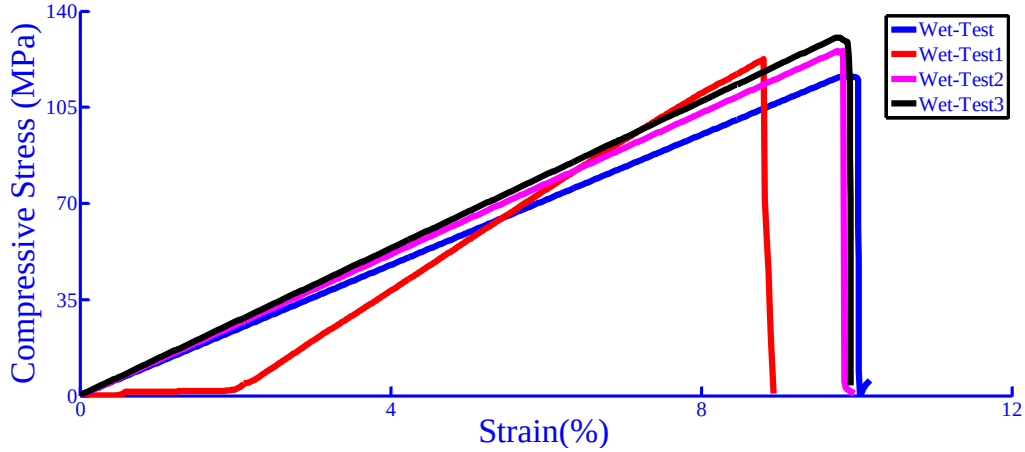

Figure 64. Wet tests for 90^o orientation at 80 °C

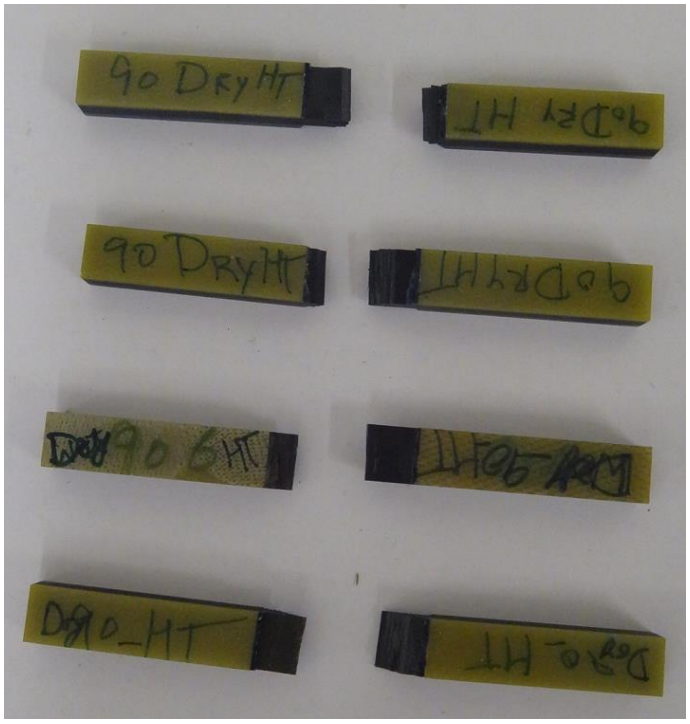

Figure 65. Failure surfaces of 90^{o} orientation specimens for dry test at 80 °C

Figure 66. Failure surfaces of 90^{o} orientation specimens for wet test at 80 °C

Table 26. Summary of test data for 90^{o} orientation at 80 °C

Test condition	**Compressive fracture load** ***kN***	**Compressive strength** ***MPa (ksi)***	**Mean** ***MPa(ksi)***
Dry	6.06	194.19(28.16)	189.09(27.43)
Dry	5.99	191.92(27.84)	
Dry	5.87	187.99(27.27)	
Dry	5.67	182.25(26.43)	
Wet	3.63	116.20(16.85)	123.68(17.94)
Wet	3.82	122.51(17.77)	
Wet	3.92	125.59(18.22)	
Wet	4.07	130.42(18.92)	

2. Analysis

2.1.1 Master storage modulus curve for dry and wet coupons

In order to derive a master curve for the dry coupons, whose individual responses are shown in Figure 1, the following expression of the storage modulus is adopted

$$\mathrm{Log}\left[E_s\left(t,T_{RT}\right)\right] = b_1^{RT}\left\{\frac{1}{2} - \frac{1}{p}\tan^{-1}\left[b_2^{RT}\left(\mathrm{Log}t - b_3^{RT}\right)\right]\right\} \quad (1)$$

where $E_s\left(t,T_{RT}\right)$ is the room temperature storage modulus after time t and b_i^{RT} are coefficients that are estimated from a least square regression performed on the experimental data; T_{RT} is the reference temperature. The resulting fit for dry coupons is also presented in Fig. 1.

The time-temperature shift principle implies that there exists a rescaled time t', also known as "reduced" time, given by

$$t' = \frac{t}{a_{RT}(T)} \quad (2)$$

where $a_{RT}(T)$ is the "horizontal" shift corresponding to the temperature T. The storage modulus at the time t' and reference temperature T_{RT} is related to the storage modulus at time t and temperature T by the following equation

$$E_s\left(t,T\right) = b_{RT}(T)E_s\left(t',T_{RT}\right) \quad (2)$$

where $b_{RT}(T)$ is the "vertical" shift factor. Hence, the values of the storage modulus at any time and temperature can be obtained from a reference curve, provided that the corresponding shift factors are known. The shift factors are determined via the regression on Eq. (1). A plot of the shift factors for the dry coupons is presented in Figure 67 and 68. Once can immediately appreciate that the application of the time-temperature shift factor to Cycom 977-2 does not require the introduction of a vertical shift, since the regression yields $b_{RT}(T)$ values very close to unity for the whole temperature range considered. The horizontal shift factor is well approximated by an Arrhenius relation with two different activation energy levels

$$a_{RT}(T) = \frac{\Delta H_1}{R}\left(\frac{1}{T} - \frac{1}{T_0}\right) \quad T \le T_1$$

$$a_{RT}(T) = \frac{\Delta H_2}{R}\left(\frac{1}{T} - \frac{1}{T_2}\right) \quad T \ge T_1 \qquad (3)$$

where $T_0 = 298.15\,\text{K}\ (25\ ^{\text{O}}\text{C})$, $T_1 = 341.8\,\text{K}\ (68.7\ ^{\text{O}}\text{C})$, $T_2 = 233.2\,\text{K}\ (-39.9\ ^{\text{O}}\text{C})$ and the activation energies are $\Delta H_1 = 68.0$ kJ/mol and $\Delta H_2 = 23.4$ kJ/mol. The fit provided by Eq. (3) is plotted in Figure 69.

In Figure 69, a sharp drop of the horizontal temperature shift is observed close to the glass transition temperature. This has to be expected, since this transition brings the material into a rubbery state that further promotes creep.

The "wet" coupons considered in this work had moisture content of about 1%. Eq. (1) is employed again to obtain time-temperature shift factors for the wet coupons. Using the data plotted in Figure 2, the regression yields again a unit value for the vertical shift factor. However, the horizontal shift factor is highly affected by the moisture content, as shown in Fig. 70. On average, the horizontal shift factor is halved by moisture content of 1% for temperatures exceeding 60°C. Below the latter temperature, the difference is larger, approaching one order of magnitude. Hence, humidity accelerates the material creep, as expected. In Figure 70, it is also worth observing that the glass transition temperature, corresponding to a sudden drop of the horizontal shift factor, decreases with the moisture content. Regarding the expression of the horizontal shift factor, Eq. (3) still holds for the coupons with 1% moisture content, but the characteristic temperatures and activation energies are: $T_1 = 317.3\,\text{K}\ (44.1\ ^{\text{O}}\text{C})$, $T_2 = 217.4\,\text{K}\ (-55.8\ ^{\text{O}}\text{C})$, $\Delta H_1 = 85.1$ kJ/mol and $\Delta H_2 = 20.1$ kJ/mol.

The reasons why a "kink" appears in the horizontal shift factor trend for $T = T_1$ is unclear. Since the 977-2 is an epoxy blended with a thermoplastic polymer for toughening purposes, it is likely that the transition temperature T_1 corresponds to a phase transition of the blend. Since the matrix formulation is proprietary, it is not possible to provide a definitive answer.

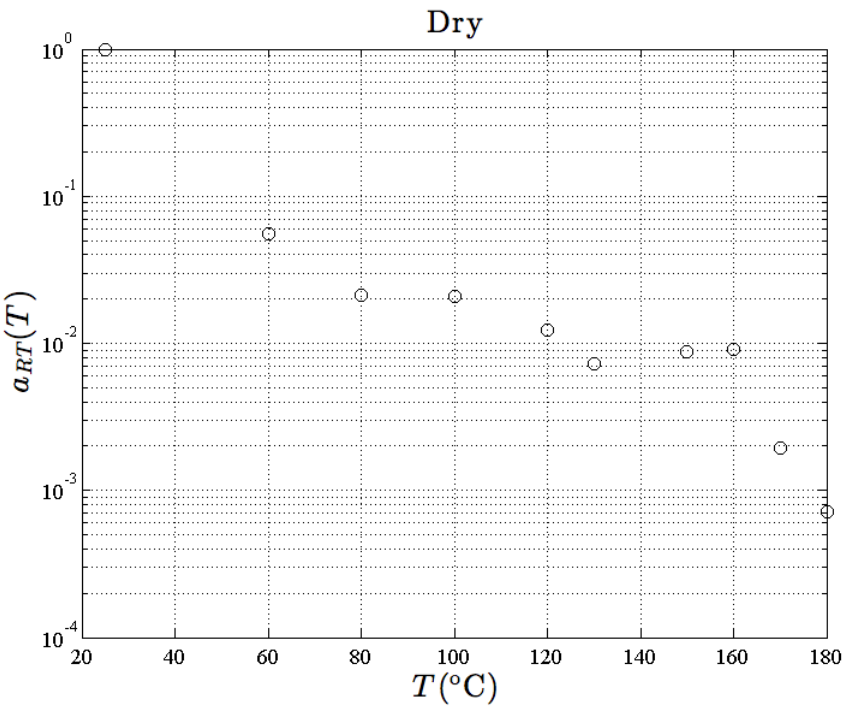

Figure 67: Horizontal time-temperature shift factor for dry coupons

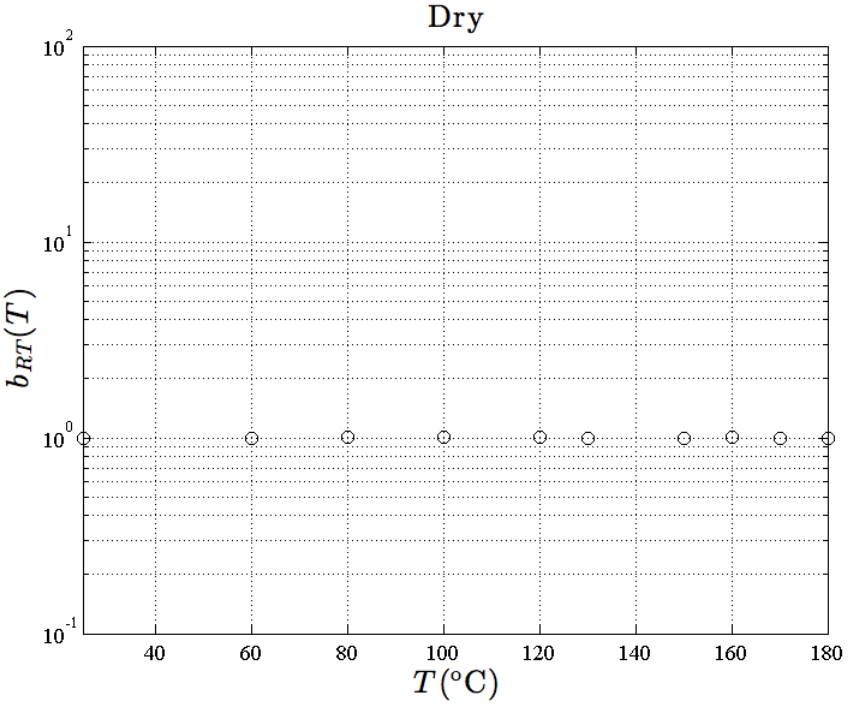

Figure 68: Vertical time-temperature shift factor for dry coupons

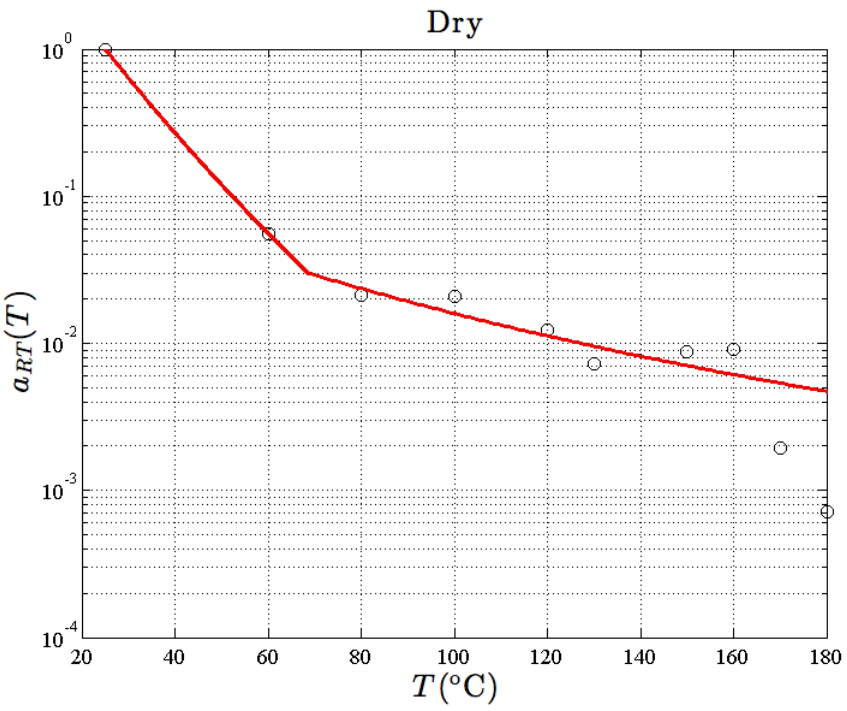

Figure 69: Fitting of horizontal shift factor via Eq. (3)

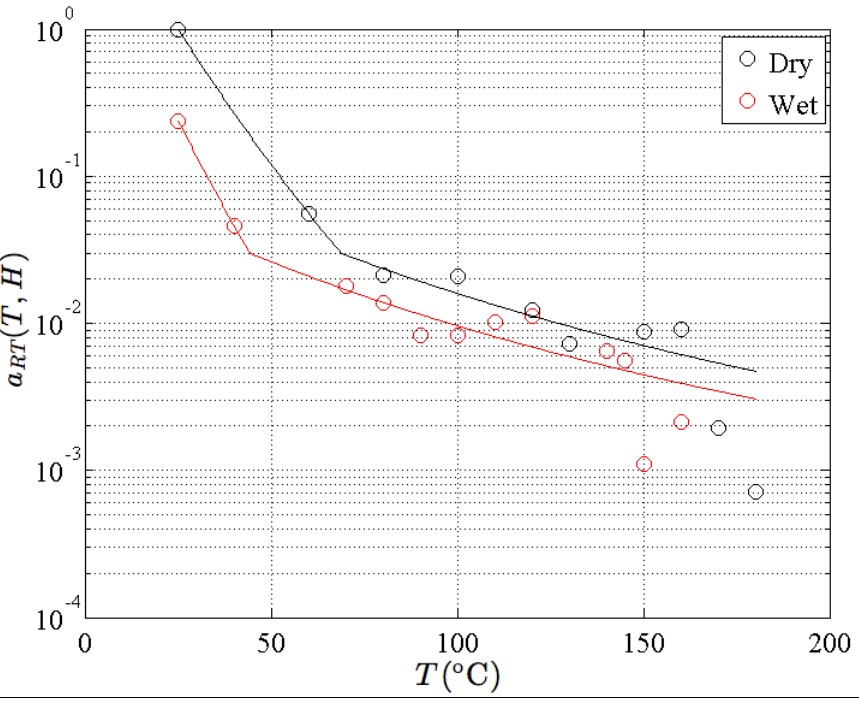

Figure 70: Horizontal shift factor for dry and wet coupons

2.1.2 Strength prediction

Regarding the strength of the unidirectional and tensile coupons, the fundamental assumptions adopted in this analysis is that the strength values can be expressed as follows

$$a_t = a_t^{RT}\left[\frac{E_s\left(t'_f, T_{RT}\right)}{E_s\left(t_f, T_{RT}\right)}\right]^g \quad (4)$$

where a_t is the strength at the temperature T and failure time t_f and a_t^{RT} is the corresponding value at room temperature for the same time to failure. The argument within square brackets is the ratio of the matrix storage modulus, which is given by the master curve; g is a characteristic exponent that depends on the strength value considered, which can be associated to tensile failure (longitudinal or transverse), compressive failure (longitudinal or transverse) and shear failure.

Therefore the procedure for validating the time temperature shift factor in terms of strength prediction is as follows:

1) Find the characteristic exponent for the strength variable of interest with respect to the RT dry value

2) Compute the reduced time from the shift factor

3) Predict the time to failure accounting for strain rate effects

4) Compare against experimental data

2.1.3 Longitudinal Tensile Strength

For the longitudinal tensile strength, micro-mechanical considerations suggest the following form for Eq. (4)

$$X_t = X_t^{RT}\left[\frac{E_s\left(t'_f, T_{RT}\right)}{E_s\left(t_f, T_{RT}\right)}\right]^{\frac{1}{2m}} \quad (5)$$

where *m* is the Weibull modulus for the IM7 fibre, which is 5.57 [14]. Figure 71 illustrates how Eq. (5) is employed to predict the longitudinal tensile strength of the composite starting from room temperature data (circles) for dry coupons. Two time shifts are required: the first accounts for the different strain rates employed in the tests (from the continuous red line to the dashed blue line); the second accounts for the different testing temperature, i.e. from room temperature to 80°C. The predicted strength lies at the intersection between the

predicted time to failure and the curve provided by Eq. (5). The predicted strength is in excellent agreement with the experimental data.

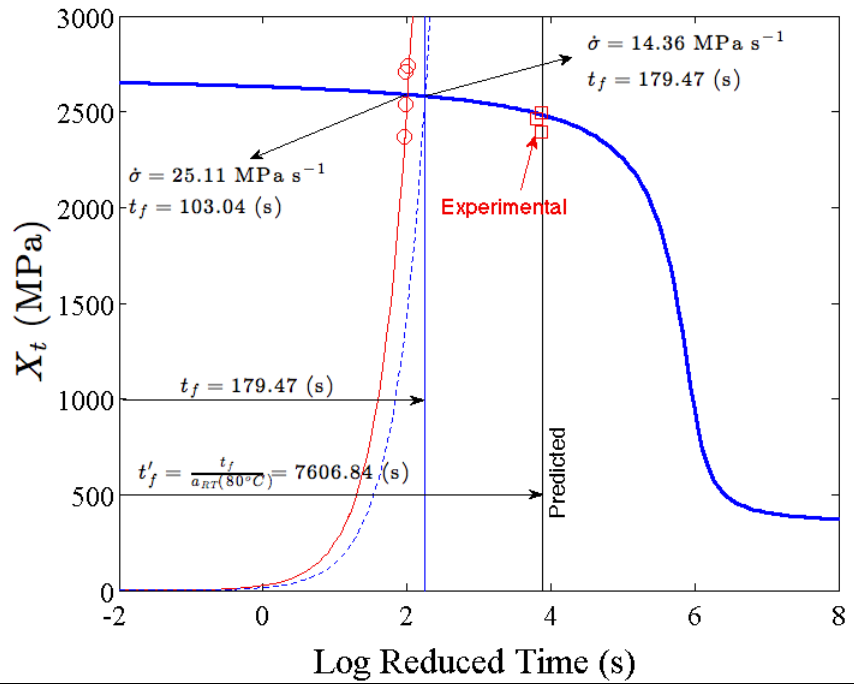

Figure 71: Longitudinal strength prediction for dry coupons

For wet ASTM coupons conditioned in water, the scenario is more complex. "Gross" moisture uptake data have been recorded for all the specimens, as outlined in Sec 1.2.2. The actual moisture level/profile in the specimen gauge section differs from that in the tabbed section, hence we adopt the definition of "gross" moisture uptake. For a through-thickness diffusivity constant of 6.45 x 10^{-8} mm^2/s, 60 days in water correspond to a 99% saturation level of the 0° unidirectional coupons (gauge section thickness of 0.82mm and bi-lateral exposure). For the other coupons, it is reasonable to assume that at least the outer plies will be fully saturated, even though a detailed modelling of the moisture uptake process should be undertaken to confirm this assumption. The moisture content in the gauge section of the 0° unidirectional coupons has been verified cutting one of the conditioned specimens and drying it in an oven at 80°C at intervals of 24 hours (5 days in total). The full saturation level corresponds to 1.8% H_2O content by weight. This moisture uptake level is higher than that reached in the DMA coupons, whose conditioning was stopped at 1% H_2O content by weight. Hence the shift factors found for the "wet" DMA coupons are not representative of the behaviour of fully saturated coupons. However, invoking the time-temperature shift principle,

the strength data for the wet 0° unidirectional coupons tested at room temperature and 80°C can be employed to estimate the horizontal shift factor by means of Eq. (5) and (2). The results of this approach are shown in Figure 72, where the horizontal shift factor is presented for three scenarios: 1) dry coupons; 2) coupons with 1% H_2O wt.; 3) fully saturated coupons (1.8% wt.). One can immediately observe that the shift factor for a 1.8% moisture content is at least one order of magnitude less than that obtained from the DMA tests for a 1% H_2O content wt. The implication of this result is that, had DMA tests been conducted on fully saturated coupons, the relaxation would have been so fast that it would have been impossible to obtain meaningful results. This points out that the shift factors associated with severe environmental degradation should be quantified by a combination of DMA and strength tests in order to obtain meaningful experimental results.

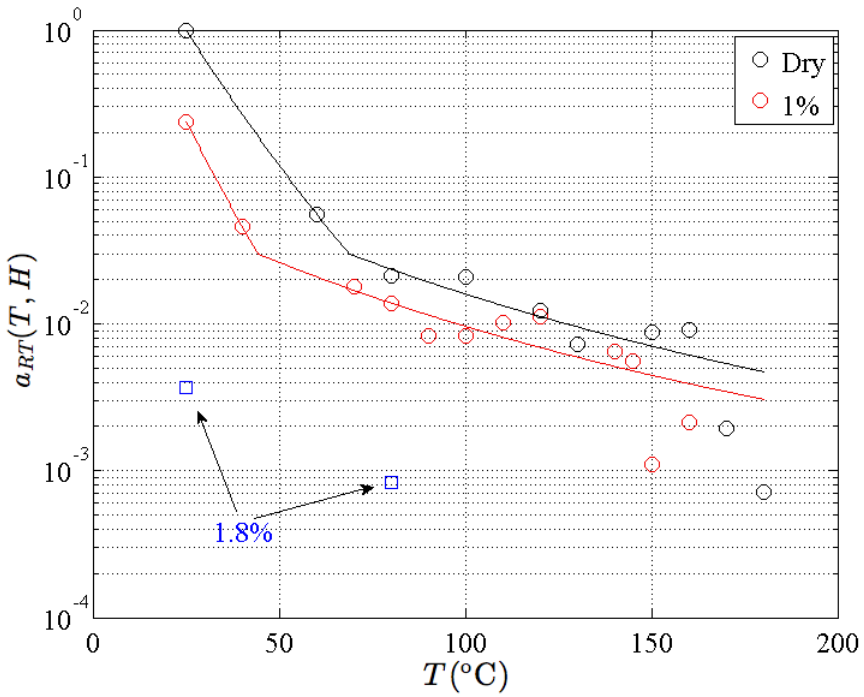

Figure 72: Horizontal shift factor for dry and wet coupons, with data for fully saturated specimens obtained from tensile tests.

2.1.4 Transverse Tensile Strength

For the transverse tensile strength of the composite, the time-temperature-humidity shift expression is:

$$Y_t = Y_t^{RT}\left[\frac{E_s\left(t'_f, T_{RT}\right)}{E_s\left(t_f, T_{RT}\right)}\right]^{\frac{1}{2}} \quad (6)$$

The exponent in Eq. (6) has been determined considering the room temperature tests performed on the dry coupons. Figure 73 shows that the Eq. (6) yields the correct strength values for the reference (calibration) case. The strength for the high temperature dry case and for the fully saturated coupons, both at room and high temperature, are presented in Figure 74-76. In all cases, Eq. (6) provides an excellent fit of the experimental data, providing a full validation of the time-temperature-humidity shift in terms of transverse strength trends.

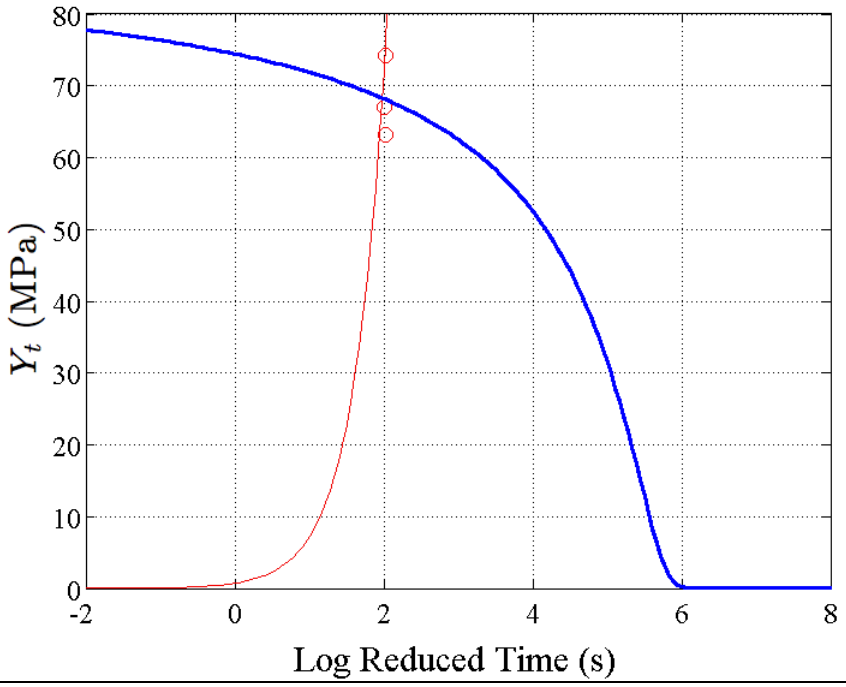

Figure 73: Calibration of Eq. (6) from experimental data; dry coupons at room temperature

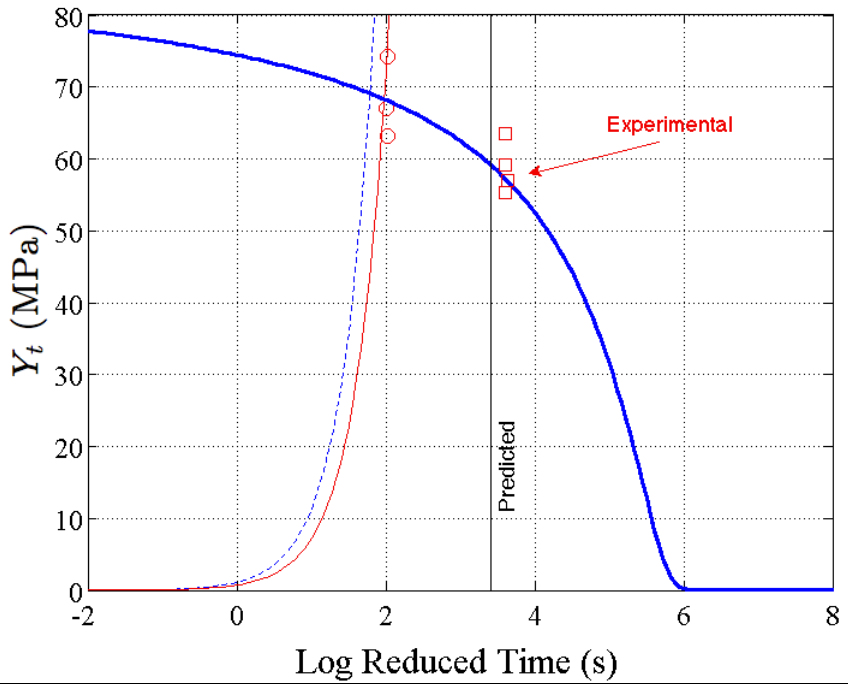

Figure 74: Transverse tensile strength prediction: dry coupons at 80°C

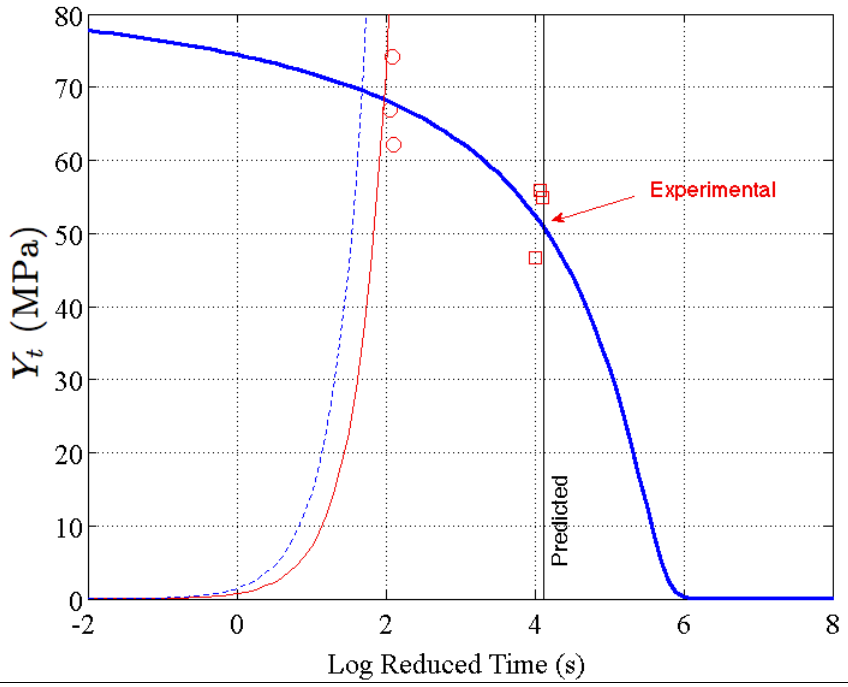

Figure 75: Transverse tensile strength prediction: fully saturated coupons at room temperature

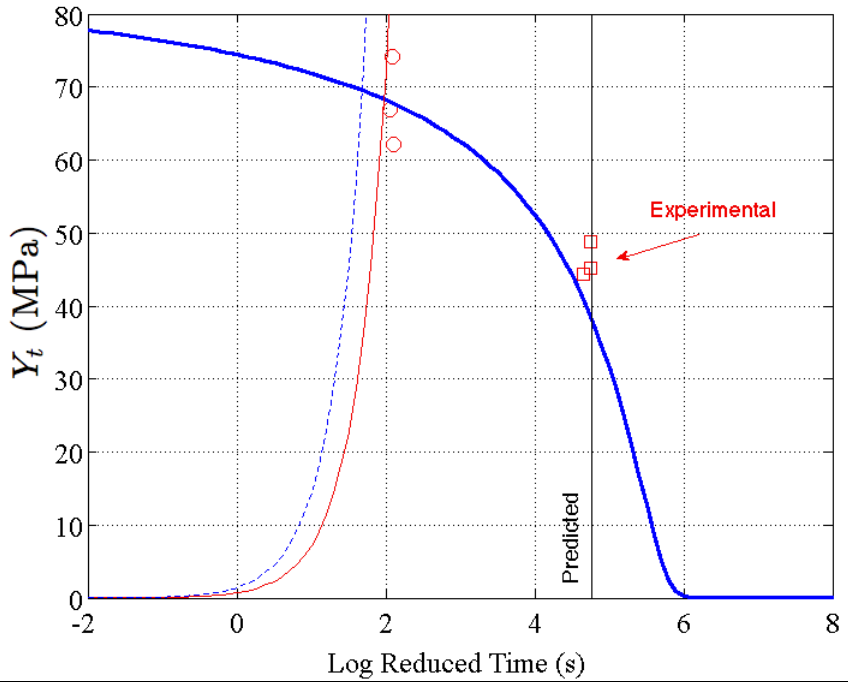

Figure 76: Transverse tensile strength prediction: fully saturated coupons at 80°C

2.1.5 Shear Strength

The in-plane shear strength of the composite has been measured via the tensile tests on the cross-ply coupons. The calibrated expression of the shear strength is given by:

$$S = S^{RT}\left[\frac{E_s\left(t'_f, T_{RT}\right)}{E_s\left(t_f, T_{RT}\right)}\right]^{0.05} \quad (7)$$

For the calibration of the shear strength given in Eq. (7), two sets of experimental data have been considered, namely at room and high temperatures. This is due to the fact that the variation of the shear strength with reduced time appears to be quite shallow and the uncertainty associated with estimating the exponent in Eq. (7) with a single set of experimental results would have been too large. The calibrated equation fits well the experimental data, as shown in Figure 77. Figure 78 and Figure 79 provide the strength values for the fully saturated coupons at room and high temperature, respectively. For the high temperature case in Figure 79, it is worth observing that the predicted strength value is conservative, i.e. the shear strength is underestimated. This is due to the fact that the shear response is visco-plastic, as demonstrated by the nonlinear load-displacement curves in Figures 46 and 47. Plastic behaviour does not conform to the time-temperature-humidity shift

factor, so the strength predictions are not as accurate as for the longitudinal and transversal tensile strength. However, the time-temperature-humidity principle provides conservative estimates, which can be useful for design purposes.

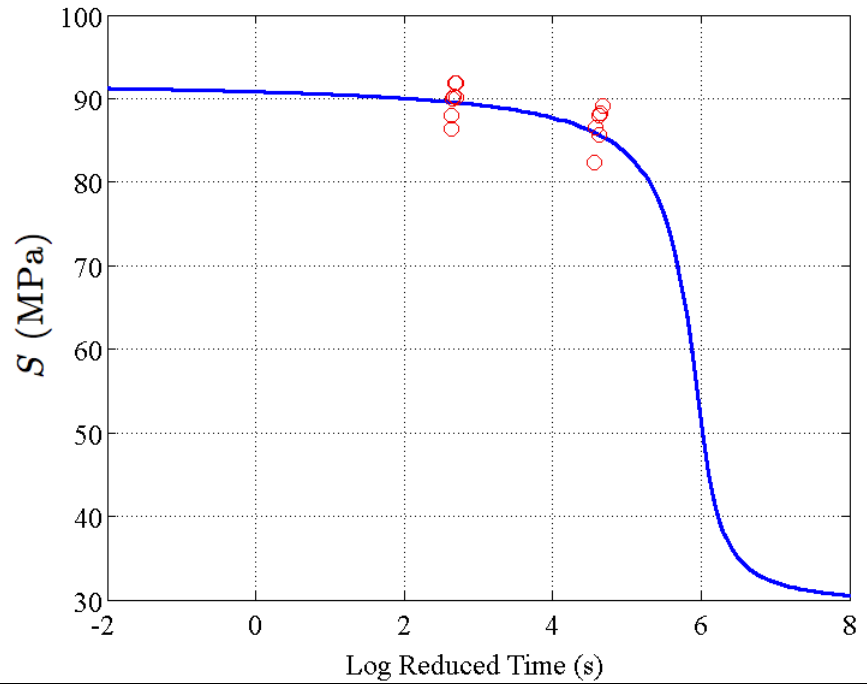

Figure 77: Calibration of Eq. (7) from experimental data; dry coupons at room temperature

3. Conclusions

The analysis presented in this section proves that:

1) The time-temperature-humidity shift principle allows estimating the effect of temperature and humidity on the longitudinal and transverse tensile strength of fibre reinforced composites.

2) The characterisation of shift factors in fully saturated coupons via creep tests (DMA) alone has proven difficult, since the loss of storage modulus with time is very fast.

3) The presence of plastic deformation invalidates the time-temperature-humidity shift principle, albeit the associated strength predictions are generally conservative.

4) The data presented in Section 1 of this report can be employed for a validation of the time-temperature-humidity shift principle for the compressive strengths of the composite. This validation has not been undertaken in the project due to lack of time cause by the delays in the material supply and recruitment of personnel.

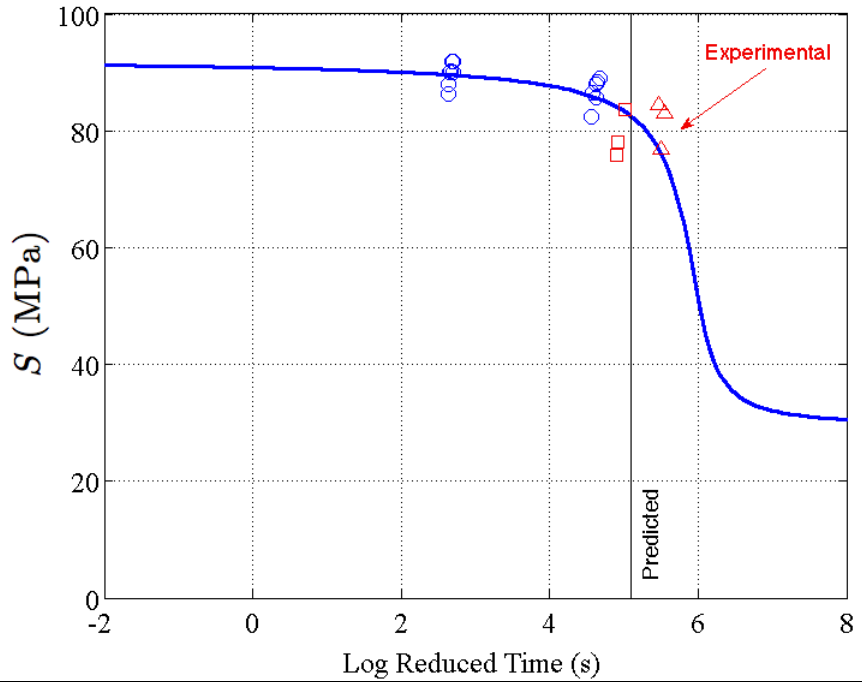

Figure 78: Shear tensile strength prediction: fully saturated coupons at room temperature

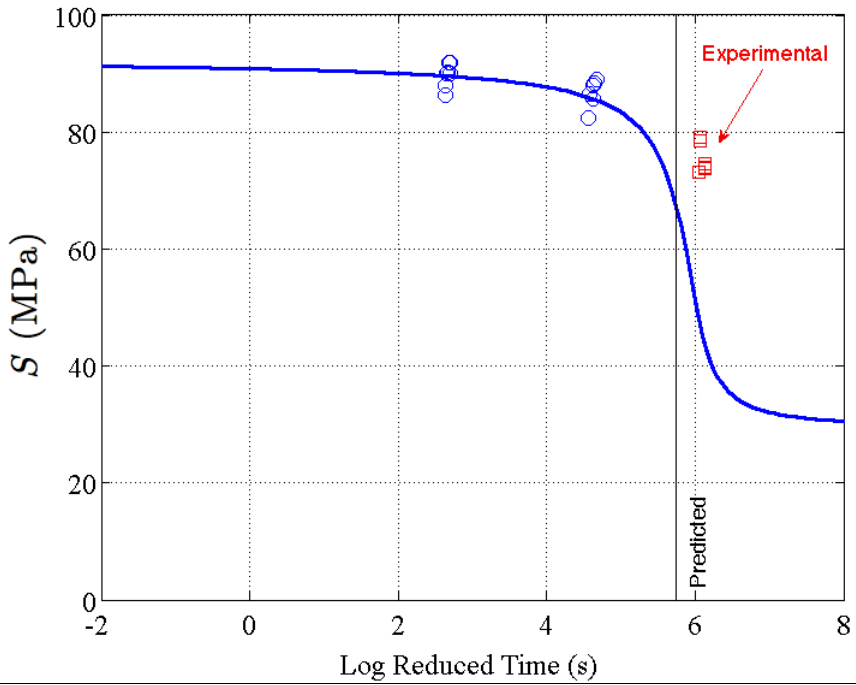

Figure 79: Shear tensile strength prediction: fully saturated coupons at at 80°C

4. Dissemination Activities

4.1 Remarks on the project results

The initial objectives of this project included: 1) the validation of the time-temperature-humidity shift principle for carbon fibre-reinforced composites; 2) the extension of the time-temperature-humidity shift principle to materials aged under cyclic humidity conditions; 3) the development of a "hydric fatigue" database, summarising the effect of cyclic moisture uptake on carbon fibre-reinforced composites. Due to several circumstances that have hindered the progress of the project, only objective 1) has been achieved. The circumstances that have contributed to this partial outcome are: 1) the fact that the consortium access agreement for CF-THREAD was signed with a 6 months delay with respect to the planned start date; 2) the fact that the material to be characterised was supplied 12 months after the planned start date; 3) delays in recruitment of research personnel. Regarding the latter, the first Research Assistant that had been appointed to carry out the research activity was not granted a work VISA in the UK. This forced the re-open the recruitment procedure. The overall delay accumulated due to the recruitment issues was a further 10 months. Hence the project effectively started 22 months late, leaving only 14 months to carry out all the planned activities. Clearly, meeting all the objectives initially stated in such short time frame was impossible. Moreover, the first coordinator of the project, Dr Alex Carrella, left the University of Bristol six months after the agreed start date and the responsibilities were handed over to Dr Giuliano Allegri. Dr Allegri also left the University of Bristol three months before the end of the grant. The delays summarised above have also impacted to original dissemination plan, whose deliverables could not be met, simply because the experimental data were generated in the last 14 months of the project and major emphasis was placed upon accelerating the project progress as much as possible. Nonetheless, a full characterisation of the in-plane material properties at different temperature and humidity levels has been undertaken. The data gathered have been employed to validate the time-temperature-humidity shift factor for a carbon-fibre reinforced composite widely employed in aerospace structures. These results provide relevant background for future attempts to extend the time-temperature-humidity shift principle to regimes involving both cyclic temperature and cyclic humidity. Ideally, it would have been extremely useful to disseminate these data during thematic conferences. Given the fact that the project has ended, the dissemination can only happen "a posteriori", aiming to publish of the data and analysis methods on high impact factor peer-reviewed journal, as summarised in Section 4.2.

4.2 Revised dissemination plan

References

[1] Reeder, J.R. (2002). "Prediction of Long-Term Strength of Thermoplastic Composites Using Time- Temperature Superposition", NASA/TM-2002-211781

[2] Haskins, J. F., J. R. Kerr and B. A. Stein. (1977). "Flight Simulation Testing of Advanced Composites for Supersonic Cruise Aircraft Applications," in *18th* 88 *AIAA/ASME Structures, Structural Dynamics & Materials Conference*, Vol. A, pp. 236-244.

[3] Ferry, J. D. 1970. *Viscoelastic Properties of Polymers*, New York: Wiley.

[4] Yeow, Y. T., D. H. Morris and H. F. Brinson. (1979). "Time-Temperature Behavior of a Unidirectional Graphite/Epoxy Composite," in *Composite Materials: Testing Design (fifth Conference), ASTM STP 674*, S. W. Tsai, Ed. Philadelphia: American Society for Testing and Materials (ASTM), pp. 263-281.

[5] Rodriquez, P. I. (1993). "On the Design of Structural Components Using Materials with Time-Dependent Properties," NASA TM108428.

[6] Miyano, Y., Kanemitsu, M., Kunio, T. and Kuhn, H. (1986). "Role of Matrix Resin on Fracture Strengths of Unidirectional CFRP", Journal of Composite Materials, 20, pp. 520-538.

[7] Miyano, Y., McMurray, M. K., Kitade, N., Nakada, M. and Mohri, M. (1994). "Role of Matrix Resin on the Flexural Static Behavior of Unidirectional Pitch-based Carbon Fiber Laminates", Advanced Composite Materials, 4, pp. 87-99.

[8] Miyano, Y., McMurray, M. K., Enyama, J. and Nakada, M. (1994). "Loading Rate and Temperature Dependence on Flexural Fatigue Behavior of a Satin Woven CFRP Laminate", Journal of Composite Materials, 28, pp.1250-1260.

[9] Miyano, Y., Nakada, M., Kudoh H. and Muki, R. (1999). "Prediction of tensile fatigue life under temperature environment for unidirectional CFRP", Advanced Composite Materials, 4, pp.235-246.

[10] Miyano, Y., Nakada, M., Kudoh H. and Muki, R. (2000). "Determination of tensile fatigue life of unidirectional CFRP specimens by strand testing", Mechanics of Time-Dependent Materials, 4, pp.127-137.

[11] Miyano, Y., Nakada, M., Watanabe, N., Murase, T. and Muki, R. (2003). "Time–temperature superposition principle for tensile and compressive strengths of unidirectional

CFRP", Proceedings of 2003 SEM Annual Conference & Exposition on Experimental and Applied Mechanics (SEM 2003), Charlotte: 147.
[12] Rosen, B.W. (1964). "Tensile failure of fibrous composites", The American Institute of Aeronautics and Astronautics (AIAA), 2, pp. 1985-1991.
[13] Rosen, B.W., Dow, N.F. and Hashin, Z. (1964). "Mechanical properties of fibrous composites", NASA contract report, pp. 31-35.
[14] NASA CR 4601, http://ntrs.nasa.gov/archive/nasa/casi.ntrs.nasa.gov/19940029731.pdf